NASA TECHNICAL NOTE

NASA TN D-6828
e. 1

NASA TN D-6828

ULTRASONIC INVESTIGATION OF THE SUPERCONDUCTING PROPERTIES OF THE Nb-Mo SYSTEM

by Lewis L. Lacy

George C. Marshall Space Flight Center
Marshall Space Flight Center, Ala. 35812

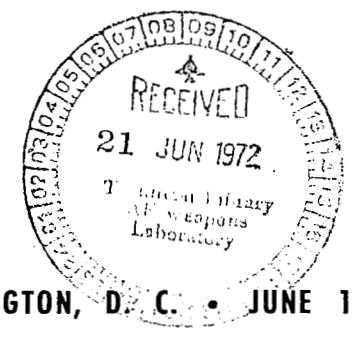

NATIONAL AERONAUTICS AND SPACE ADMINISTRATION • WASHINGTON, D. C. • JUNE 1972

1. Report No.	2. Government Accession No.	3. Recipie.
NASA TN D-6828		

4. Title and Subtitle	5. Report Date
Ultrasonic Investigation of the Superconducting Properties of the Nb–Mo System	June 1972
	6. Performing Organization Code
7. Author(s)	8. Performing Organization Report No.
Lewis L. Lacy	
	10. Work Unit No.
9. Performing Organization Name and Address	
George C. Marshall Space Flight Center Marshall Space Flight Center, Alabama 35812	11. Contract or Grant No.
	13. Type of Report and Period Covered
12. Sponsoring Agency Name and Address	Technical Note
National Aeronautics And Space Administration Washington, D.C. 20546	14. Sponsoring Agency Code

15. Supplementary Notes

Prepared by Space Sciences Laboratory, Science and Engineering

16. Abstract

The superconducting properties of single crystals of Nb and two alloys of Nb with Mo have been investigated by ultrasonic techniques. The results of measurements of the ultrasonic attenuation and velocities as a function of temperature, Mo composition, crystallographic direction, and ultrasonic frequency are reported. The attenuation and small velocity changes associated with the superconductivity of the samples are shown to be dependent on the sample resistivity ratio Γ which varied from 4.3 for Nb-9% Mo to 6500 for pure Nb.

The ultrasonic attenuation data are analyzed in terms of the superconducting energy gap term $2\Delta(0)/kT_c$ of the BCS theory. A new model is proposed for the analysis of ultrasonic attenuation in pure superconductors with two partially decoupled energy bands. To analyze the attenuation in pure superconducting Nb, the existence of two energy gaps was assumed to be associated with the two partially decoupled energy bands. One of the gaps was found to have the normal BCS value of 3.4 and the other gap was found to have the anamalously large value of 10. No experimental evidence was found to suggest that the second energy gap had a different transition temperature.

The interpretation of the results for the Nb-Mo alloys is shown to be complicated by the possible existence of a second superconducting phase in Nb-Mo alloys with a transition temperature T_{c2} of 0.35 of the transition temperature T_{c1} of the first phase.

The elastic constants of Nb and Nb-Mo alloys are shown to be approximately independent of Mo composition to nine atomic percent Mo. These results do not agree with the current microscopic theory of T_c for the transition elements.

17. Key Words (Suggested by Author(s))	18. Distribution Statement

19. Security Classif. (of this report)	20. Security Classif. (of this page)	21. No. of Pages	22. Price*
Unclassified	Unclassified	53	$3.00

* For sale by the National Technical Information Service, Springfield, Virginia 22151

TABLE OF CONTENTS

		Page
SECTION I.	INTRODUCTION	1
SECTION II.	ATTENUATION MEASUREMENTS	4
	A. Experimental Technique	4
	B. Results of the Normal Electron Attenuation	8
	C. Results of Superconducting Attenuation in Nb[100]	10
	D. Model for α_s/α_n in Pure Nb	16
	E. Attenuation Results for Nb-Mo Alloys - Evidence for a Second Energy Gap in Nb-Mo Alloys	18
	F. Summary of Attenuation Results	24
SECTION III.	VELOCITY MEASUREMENTS AND ELASTIC CONSTANTS	26
	A. Absolute Velocity Measurements	26
	B. Elastic Constants	30
	C. Small Velocity Changes Associated with Superconducting Properties of Nb-Mo Alloys	34
SECTION IV.	CONCLUSIONS	38
APPENDIX A:	METHOD USED TO CALCULATE α_s/α_n	40
APPENDIX B:	MATERIAL CHARACTERIZATION	42
APPENDIX C:	POSSIBLE SOURCES OF ERROR FOR ATTENUATION EXPERIMENT	45
APPENDIX D:	APPARENT VELOCITY CHANGES DUE TO ATTENUATION CHANGES	47
REFERENCES		48

LIST OF ILLUSTRATIONS

Figure	Title	Page
1.	The usual temperature dependent ultrasonic attenuation in a pure superconductor	2
2.	Schematic for ultrasonic attenuation experiment	5
3.	Oscilloscope traces for a typical echo pattern at three different temperatures for Nb [100]	6
4.	Sample holder with sample	7
5.	Comparison of exponential and nonexponential decay	9
6.	Normal electron attenuation as a function of ultrasonic frequency	11
7.	Reduced normal electron attenuation as a function of reduced temperature	12
8.	Superconducting and normal electron attenuation in Nb[100]	13
9.	Effective energy gap in Nb[100]	14
10.	Superconducting attenuation in Nb[100] showing that the anomalous results are independent of $q\ell_e$	17
11.	Superconducting attenuation in Nb-9%Mo[110]	19
12.	Effective energy gap for two Nb-Mo alloys	20
13.	Superconducting and normal electron attenuation in Nb-5%Mo[100]	22
14.	Superconducting attenuation in Nb-9%Mo[110] after defining T_{c2}	23
15.	Energy gaps experimentally observed in Nb and Nb-Mo alloys as a function of temperature	25
16.	Schematic for ultrasonic velocity experiment	27
17.	Method for measuring the phase shift at the transducer-sample interface τ_{pt}	31
18.	Fractional change in ultrasonic transit time for Nb[110] as a function of temperature	35
19.	Fractional change in ultrasonic velocity for Nb-9%Mo[110] as a function of temperature	36
B-1.	Percent change in resistivity for Nb-Mo single crystals as a function of Mo compositions	43

LIST OF TABLES

Table	Title	Page
1.	Measured Transit Times for Nb-5%Mo [100] 46 MHz Longitudinal (4.2 K)	29
2.	Elastic Constants of Nb and Nb-9%Mo	33
B-1.	Resistivities and T_c of Nb and Two Alloys of Nb-Mo	42

ACKNOWLEDGMENTS

The author would like to express his sincere appreciation to Dr. Stan Sekula and Dr. Richard Reed of the Oak Ridge National Laboratory for several of the Nb and Nb–Mo single crystals which made this investigation possible. He would also like to note the many useful discussions with the following people: Dr. Eugene Urban of MSFC, Dr. Alfred Daniel of the U.S. Army Missile Command, Dr. J. O. Thomson of the University of Tennessee, and Dr. Guenther Otto of the University of Alabama Research Institute.

ULTRASONIC INVESTIGATION OF THE SUPERCONDUCTING PROPERTIES OF THE Nb-Mo SYSTEM

SECTION I. INTRODUCTION

Superconductivity is an exciting and mysterious field which has challenged scientists and engineers for three generations. Besides superfluidity, it is the only macroscopic manifestation of quantum mechanics. The superconducting state is considered an ordered quantum state of the conduction electrons of the metal. The electrons responsible for superconductivity are weakly bound in ordered pairs below some critical or transition temperature, T_c, below which a superconductor loses all dc electrical resistance. For temperatures above T_c the electrons become disordered and behave as electrons in a normal metal.

The first comprehensive microscopic theory of superconductivity was published by Bardeen, Cooper, and Schrieffer (BCS) [1] who provided an explanation for both the measured equilibrium properties such as specific heat and the nonequilibrium properties such as microwave absorption and ultrasonic attenuation. The BCS theory assumed that the conduction electrons interact with each other and form bound pairs through the exchange of lattice phonons. The superconducting bound pairs, often called Cooper pairs, form the ground state for a superconductor. At absolute zero temperature, all conduction electrons are in the superconducting ground state which is separated from the conduction band by an energy gap $\Delta(0)$. At a finite temperature between absolute zero and T_c, the superconductor contains three electronic components: The ground state superconducting pairs and thermally excited states occupied either singly or in pairs similar to the situation in the normal metal. The thermally excited states must have energies greater than the temperature dependent energy gap $\Delta(T)$. For direct ultrasonic or electromagnetic excitation, a minimum energy of $2\Delta(T)$ must be applied to the superconducting ground state pairs to excite them into the conduction band.

Ultrasonic attenuation experiments by Bömmel [2] on Pb and by Mackinnon [3] on Sn had preceded the BCS theory by 2 years and had shown that ultrasonic waves are absorbed by the conduction band electrons. The absorption mechanism can be thought of in terms of a deformation of the crystal lattice, where the electrons try to follow the deformation and in the process absorb or create phonons with a corresponding change in the momentum of the electrons. Figure 1 shows a typical result of the way sound is absorbed in a pure superconducting metal. The background attenuation is usually independent of temperature, but the attenuation due to the electrons increases because of the increase in the electron's mean free path ℓ_e which increases at low temperatures because of less scattering from thermal phonons (curves a and c). The normal electron attenuation α_n usually approaches a limiting value when ℓ_e is limited by impurity scattering in the metal. The ultrasonic wave is still absorbed at intermediate temperatures in a superconductor (curve b) due to the thermally excited electrons above the superconducting energy gap $\Delta(T)$. The electronic contribution to the ultrasonic attenuation vanishes at low temperatures since all the electrons are in the superconducting ground state. Because the energy of the phonons associated with ultrasonic waves is much less than the energy gap, the observed acoustic response samples only the thermal excitation spectrum in the conduction band of the superconductor, where the thermal excitation spectrum is specified by the Fermi function $f(\Delta/T)$.

The BCS theory provided the basic equation governing the ultrasonic attenuation observed by Bömmel and Mackinnon

$$\alpha_s/\alpha_n = 2f(\Delta/T) = 2/\{\exp\ [\Delta(T)/kT] + 1\}, \qquad (1)$$

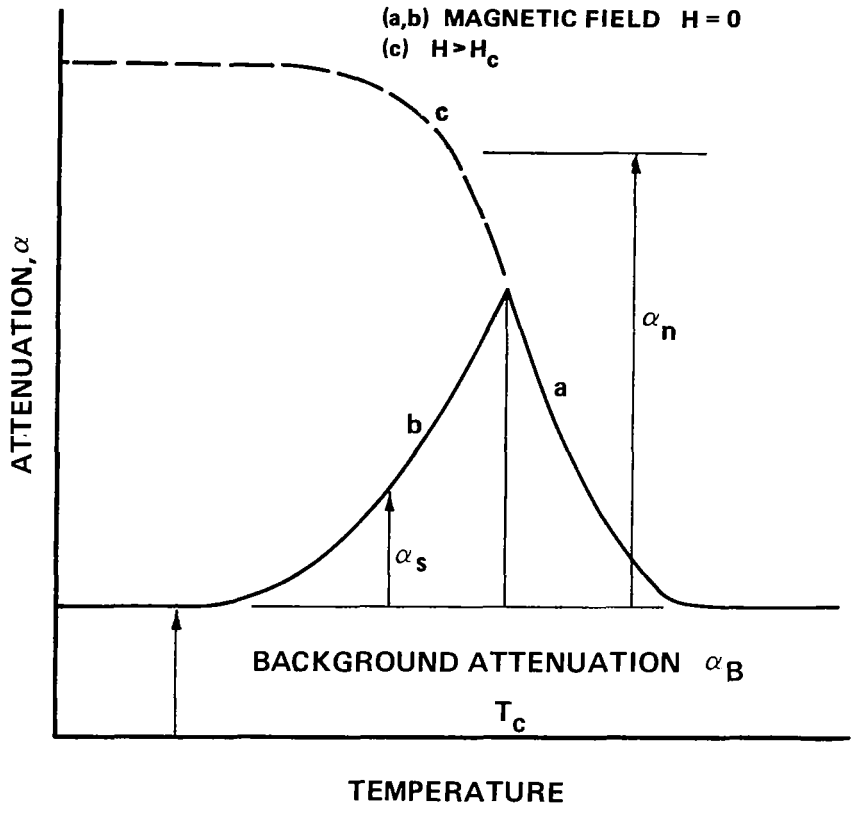

Figure 1. Usual temperature dependent ultrasonic attenuation in a pure superconductor.

where α_s is the attenuation when the electrons are superconducting and α_n is the attenuation for normal electrons. Longitudinal ultrasonic attenuation is governed only by the absolute temperature and the temperature dependent energy gap. The normalized energy gap $\Delta^* = \Delta(T)/\Delta(0)$ was found in the BCS theory to be a function only of the reduced temperature $t = T/T_c$ for all superconductors. The BCS theory also showed that the ratio $2\Delta(0)/kT_c$ in the weak coupling limit is a constant for all superconductors with a value of 3.52. Typical BCS curves of Δ^* and α_s/α_n will be presented in Section II.

Equation (1) was originally derived for an isotropic, weakly coupled ($T_c/\theta_D \leq 0.01$) superconductor with $q\ell_e >> 1$, where q is the ultrasonic wave number and θ_D the Debye temperature. Kresin [4] extended equation (1) to the case $q\ell_e << 1$, and Tsuneto [5] showed that it should be valid for all $q\ell_e$. Calculations by Ambegaokar [6] showed that the same equation should apply for the strongly coupled superconductors when $q\ell_e >> 1$.

Equation (1) has been experimentally tested with hundreds of experiments using most of the known pure superconductors in the periodic table. In general, the experimental results tend to agree with the theory, except for somewhat smaller attenuation (1 to 5 percent) for temperatures near T_c.

The first ultrasonic attenuation measurements [7, 8] on superconducting Nb agreed with equation (1). Using shear waves with $q\ell_e < 1$, Levy [7] obtained reasonably good agreement between his data on Nb[110] and the BCS theory by assuming the energy gap at absolute zero $\Delta(0)$ to be given by $A \equiv 2\Delta(0)/kT_c = 3.6$ to 4.0. Small departures from theory for $0.3 < t < 0.8$ were not discussed by Levy but will be shown in this report to be due to the purity of his sample. Weber [8] obtained excellent agrement with theory for Nb samples with longitudinal waves and $q\ell_e \sim 1$ along the principal symmetry axes by using energy gaps of $A = 3.63 \pm 0.06$. Ikushima [9] found reasonable agreement with the BCS theory for longitudinal waves and $A \approx 3.5 \pm 0.1$.

Perz [10] was the first to report any significant deviations from the BCS theory. The energy gap of his samples at T = 0 was approximately the same as previously reported ($A \approx 3.5$ to 3.8), but he noted two additional effects:

1. A decreases as $q\ell_e$ increases.

2. The energy gap $\Delta^* \equiv \Delta(T)/\Delta(0)$ deviated significantly from the BCS value for $0.3 < t < 0.9$.

Tsuda [11], independently and at approximately the same time, also reported deviations from the BCS theory for a polycrystalline sample of Nb with longitudinal waves and $q\ell_e << 1$. His results seem to fit a BCS type curve with A = 4.4 for $t \approx 1$ and another BCS type curve with A = 3.5 for $t \leqslant 0.4$. In a subsequent paper, Tsuda [12] showed that the observed deviations were related to the purity of his samples as expressed by the resistivity ratio $\Gamma \equiv R_{300}/R_4$. Previously reported BCS behavior was found for $\Gamma \approx 200$, but for $\Gamma \gtrsim 400$ non-BCS behavior was observed.

A report on the ultrasonic attenuation measurements of high purity Nb and two alloys with Mo is included in Section II. It will also be shown that the results on pure Nb[100] agree with the measurements reported by Perz and Tsuda and that these results combined with those of Levy, Weber, Perz, and Tsuda demonstrate that the measured energy gap in Nb depends strongly on the value of ℓ_e but is probably independent of $q\ell_e$. It will then be shown that the attenuation results for Nb can be understood in terms of two energy gaps, and finally, the impact of these measurements on the BCS theory and the need for a modified BCS theory to explain values of $A > 4.0$ will be discussed.

Attenuation results for Nb-9%Mo[110] and Nb-5%Mo[100] will also be reported. It will be shown that due to two other effects it is difficult to interpret the results of Nb-Mo alloys in terms of a simple energy gap. The resonance effect has been studied previously and the other effect, a second superconducting phase, suggests a new application of ultrasonics in the study of the superconducting properties of alloy superconductors.

Alloys of Nb-Mo were chosen for this study because of the following three criteria:

1. Nb is a strongly coupled superconductor with the highest transition temperature (9.2 K), while Mo is a weakly coupled superconductor with a low transition temperature (0.9 K). Alloys of Nb and Mo have a linear relationship between T_c and Mo composition. It was hoped that some insight could be gained concerning the deleterious effects on Nb of small amounts of Mo.

2. Previous measurements, such as specific heat and lattice constants, had been made on the Nb-Mo system. Thus, ultrasonic measurements in Nb-Mo can be compared and analyzed in terms of other results.

3. Nb and Nb-Mo alloys are borderline Type II superconductors. A study of these materials could assist in determining whether or not Type II superconductors differ basically from Type I superconductors in their microscopic properties. Preliminary magnetic results for very pure Nb indicate that pure Nb may be approaching the limit which separates Type I and Type II superconductors.

As a parallel study to the attenuation measurements on the Nb-Mo system, the velocities of sound and corresponding elastic constants of the Nb-Mo system were accurately measured. It was hoped that these measurements could be correlated with the superconducting properities of the system, since the theories of McMillan [13] and Hopfield [14] indicated that a strong correlation should exist. The measurements indicated that no significant correlation exists, and that either there is a basic weakness in the theory or that much higher frequencies not available to ultrasonic techniques must be considered.

Finally, this study reports on the extremely small changes in the velocity of sound or elastic constants associated with the superconducting transitions of Nb and Nb-9%Mo. Although no theory exists to explain these data, measurements of small velocity changes in superconductors have been previously reported. Deaton [15] has recently reported measurements on Pb[110] and Yee [16] on Sn. This study indicates that extreme care must be used in interpreting the results of such ultrasonic velocity measurements due to apparent velocity changes caused by the attenuation in the sample. An equation will be derived to relate the observed velocity changes to the observed attenuation changes.

SECTION II. ATTENUATION MEASUREMENTS

A. Experimental Technique

The ultrasonic attenuation of samples of pure Nb, Nb-5%Mo, and Nb-9%Mo was measured using the pulse-echo technique. Radio frequency pulses of 2 to 4 μs duration and 10 to 50 MHz frequency are impressed across an X-cut quartz transducer bonded to the flat end face of a cylindrical sample. The pulsed rf electric field produces an ultrasonic pulse that passes into the specimen. The same quartz transducer is used to detect the ultrasonic echo pattern produced by the repeated reflection of the sound between the two parallel end faces. A schematic of the electronics used to determine the attenuation as a function of temperature is illustrated in Figure 2. The ultrasonic attenuation was determined by measuring the amplitude of a selected echo with a boxcar integrator. The analog averaging technique of the boxcar integrator increases the signal-to-noise ratio of the measurement and allows measurement of very small changes in attenuation. We have measured relative changes in attenuation of 1×10^{-4} dB/cm using the technique reported here.

Oscilloscope tracings of typical echo patterns for three different temperatures are shown in Figure 3 where the numbers at the top of each picture refer to the scale setting of the oscilloscope. The tracings in the center of each photograph show the first echo with an expanded time scale (500 ns/cm). Figures 3A and 3B show the increase in normal electron attenuation as the temperature of the sample is decreased to T_c. Figure 3C shows the decrease in the electronic contribution to the attenuation when the sample is cooled to 4.2 K. The gate of the boxcar integrator is also shown in Figure 3.

A schematic of the sample holder used in the experiments is shown in Figure 4. The sample holder consists of a copper cylinder containing the sample, a germanium thermometer, a constantan heater, and a carbon temperature control thermometer. The entire sample holder is contained in an evacuated copper can (0.1 Torr), since earlier measurements had shown the unreliability of attenuation data taken at atmospheric pressure. Each sample was fitted with a different machined copper cylinder to help insure good thermal contact between the sample and the copper sample holder. Also to help minimize thermal gradients across the sample, all leads to the sample holder were thermally grounded to the outside copper can.

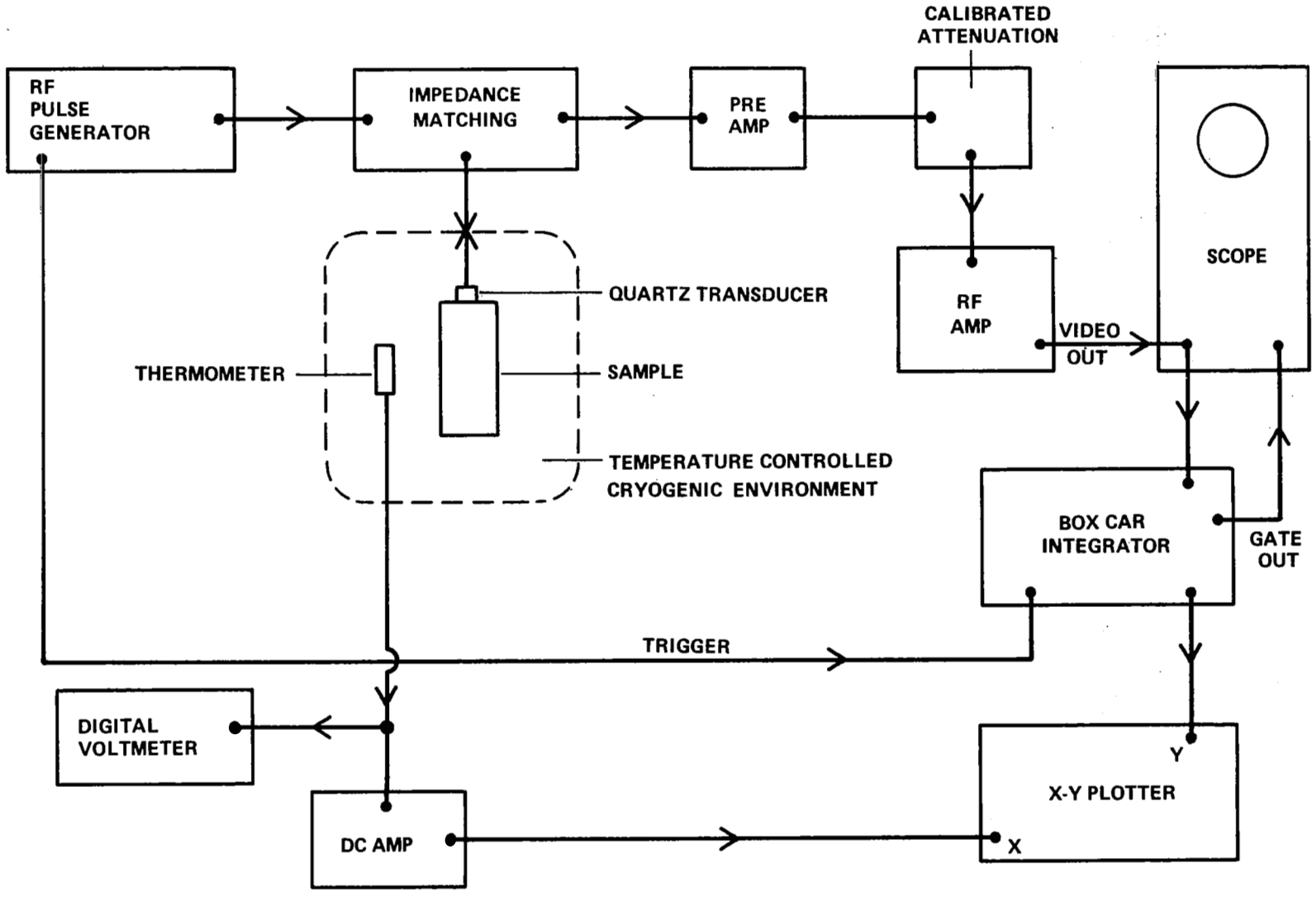

Figure 2. Schematic for ultrasonic attenuation experiment.

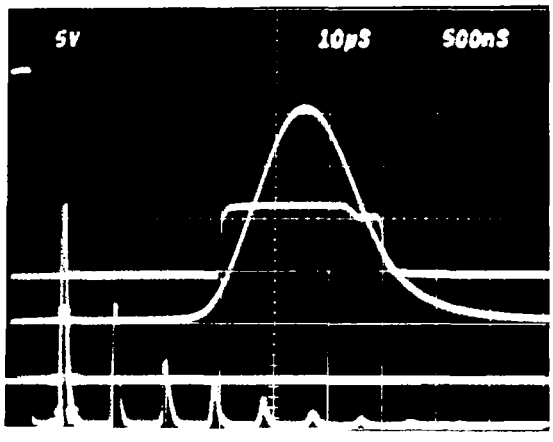

A. T = 18 K

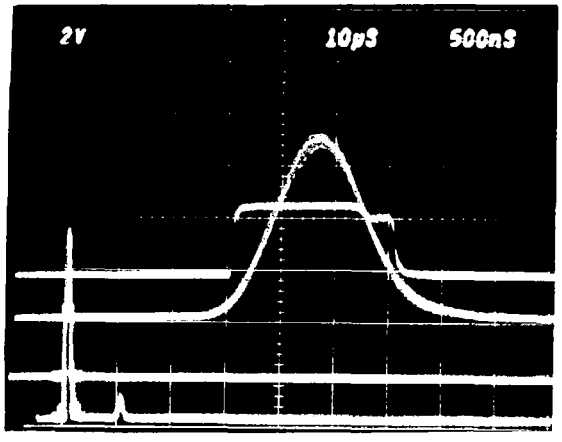

B. T ≈ T_c = 9.2 K

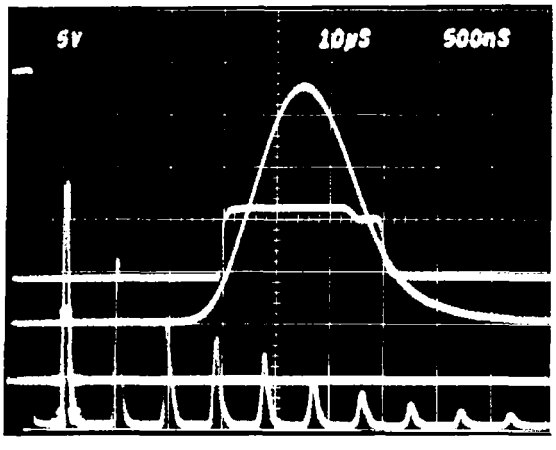

C. T = 4.2 K

Figure 3. Oscilloscope traces for a typical echo pattern at three different temperatures for Nb [100].

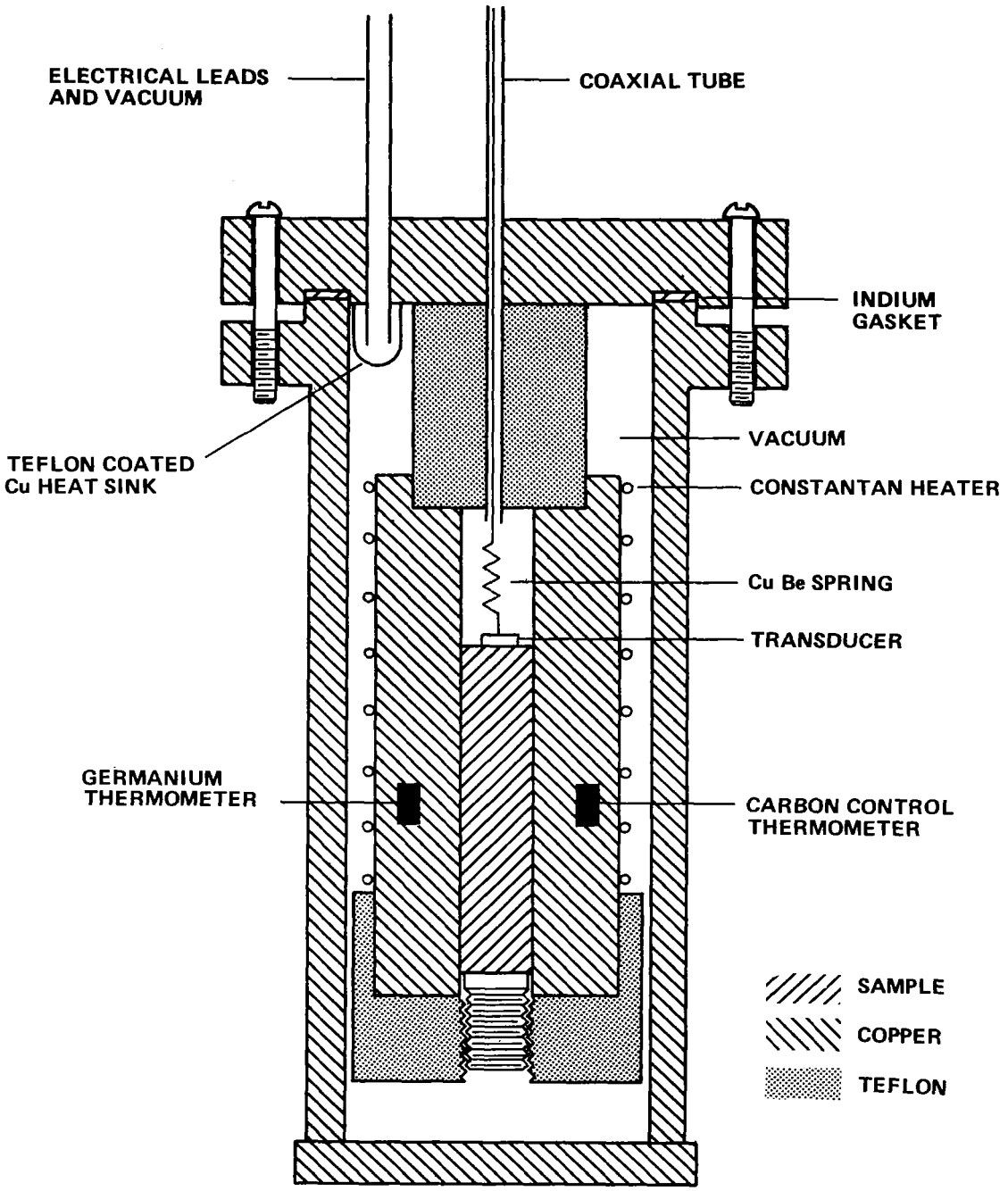

Figure 4. Sample holder with sample.

The temperature of the sample was measured by a germanium resistance thermometer calibrated with respect to a secondary standard provided by the Oak Ridge National Laboratory. The calibration curve is believed to be correct to within 2 mK.

The samples were oriented to within ±1 degree of their principal axis using the Laue X-ray technique. After orientation, the end faces of the samples were polished flat and parallel to within 2 seconds of arc. After polishing, no evidence of surface damage could be detected by X rays; however, examination with a microscope revealed several small scratches of 1 μm widths. No evidence of pits or voids could be optically or acoustically detected ($\lambda \approx 0.01$ cm).

X-cut quartz transducers of 5 and 10 MHz fundamental frequency were bonded to the surface of the crystals using Dow Corning 200 silicone fluid with a viscosity of 60×10^3 centistokes. To help minimize diffraction and end effects, the diameters of the quartz transducers were all less than the diameters of the samples. After the samples were cooled to liquid nitrogen temperature, the ultrasonic echo patterns were found to be exponential. An example of exponential decay in Figure 5A can be compared with an example of nonexponential decay in Figure 5B for the same sample. The nonexponential decay seen in Figure 5B was caused by a scratch 20 μm wide across the polished surface of the example. Evidently, the small scratch on the sample's surface greatly intensifies the diffraction losses in the sample. No measurements were made when the decay pattern was found to be nonexponential.

A typical experiment consisted of plotting on an X-Y recorder the height of a selected echo as a function of resistance of the germanium thermometer. The temperature of the sample was slowly increased from 4.2 K to about 10 K at an average rate of about 1 mK/s using a commercial temperature controller. The above procedure was then repeated for decreasing temperature. Several times during each experimental run, a sensitive digital voltmeter was used to accurately measure the resistance of the germanium thermometer. In this manner, any nonlinearity ($\approx$ 1 percent) of the dc amplifiers could be checked. Also if any nonlinear effects of the rf amplifiers were suspected during the course of an experiment, the above procedure was repeated for a different echo or for a different gain of the rf amplifier.

The normal-state electron attenuation α_n was measured by repeating the above measurements while the sample was in a magnetic field $H > H_{c2}$ (4.2 K). As a final experiment, the superconducting electron attenuation α_s was measured for $T < 4.2$ K by pumping on the liquid helium. The method used to calculate both the normal and superconducting attenuation is given in Appendix A.

B. Results of the Normal Electron Attenuation

Using the concept of a viscous electron gas attenuating sound, Mason [17] has shown that the normal-state electron attenuation for longitudinal waves α_n is given by

$$\alpha_n = \frac{2}{15}\frac{Nmv_F}{\rho v_L^3}\,\omega^2 \ell_e \qquad (q\ell_e < 1) \quad , \tag{2}$$

where N is the electron number density and ω is the ultrasonic frequency; m, v_F and ℓ_e, respectively, are the free-electron mass, the Fermi velocity, and the electron mean free path; ρ is the material density; and v_L is longitudinal velocity of sound. A good discussion of normal electron attenuation can be found in Reference 18.

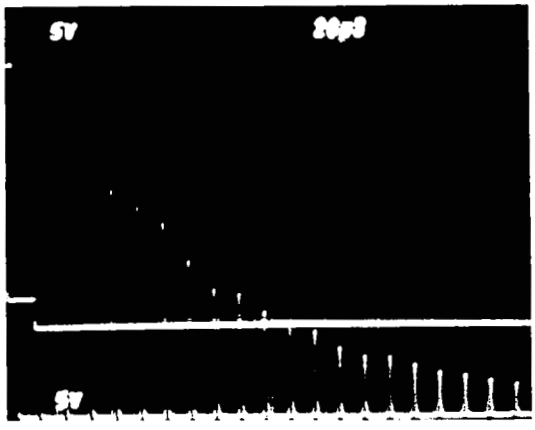

A. Normal exponential decay pattern Nb [110] 30 MHz long.

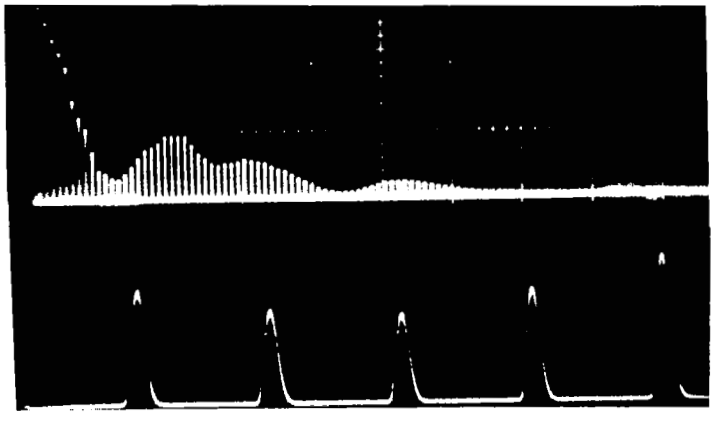

B. Severe diffraction losses Nb [110] 50 MHz long.

Figure 5. Comparison of exponential and nonexponential decay.

For all samples and frequencies, $q\ell_e$ was much less than unity except for the case of the very pure Nb[100] sample where $q\ell_e$ was of the order of unity. The electron mean free path ℓ_e was estimated for these samples by measuring their resistivity ratio Γ. The method used to measure Γ and calculate ℓ_e is given in Appendix B where other material characterizations such as T_c and impurity content are also reported. Since ℓ_e is proportional to α_n, the ratio of α_n for Nb[110] and Nb-9%Mo[110] was found to be equal to the ratio of their respective Γ. Although Γ of Nb[100] could not be measured directly by dc methods, Γ was estimated to be 6500 by using the ratio of α_n for Nb[100] and Nb-5%Mo[100]. This compares favorably to the values of 6000 to 7500 obtained by Sekula[1] for the same material using the eddy current technique. Thus, this Nb sample has a resistivity ratio approximately 10 times greater than any Nb for which acoustical measurements have previously been reported.

In Figure 6, α_n is plotted as a function of frequency ω for Nb-9%Mo. From the slope of the straight line, α_n is seen to be proportional to ω^m, where $m = 2.0 \pm 0.1$ for $q\ell_e \ll 1$. The two attenuation measurements on Nb have also shown a ω^2 dependency for $q\ell_e \approx 1$. Therefore, the validity of equation (2) for the Nb-Mo system for the two main variables ω and ℓ_e have been shown. It is indeed remarkable that for a complicated s and d band structure of Nb, a free electron model holds for a 600-fold change in ℓ_e (i.e., from the extreme case of impurity-limited scattering in the "dirty" superconductor Nb-9%Mo to the other extreme case of phonon-limited scattering of very pure Nb).

Since α_n is proportional to ℓ_e, a plot of α_n versus temperature provides a method of studying ℓ_e versus temperature (at least for $q\ell_e < 1$). In Figure 7, α_n for Nb[100] normalized to $\alpha_n(T = T_c)$ is plotted for $0.5 \leqslant t \leqslant 1.5$. As seen from the slope of the straight lines, ℓ_e is proportional to t^n with $n = -3.2$ for $t \geqslant 1$ and $n = -1.6$ for $t < 1$. The discontinuity in the slope at $t = 1$ is due to the decrease in ℓ_e with the application of a magnetic field parallel to $\vec{q}$.

The T^3 behavior of Nb is very different from the Bloch T^5 law for the low-temperature electrical resistivity of simple metals. Recently, Kaveli [19] has criticized the Bloch theory even for the simple metals, such as Na. Also, recently, Campbell [20] has derived a T^3 behavior for alloys. His argument is based on the nonconservation of momentum for electrons scattering from phonons in the dirty limit of an alloy. The data derived for this report indicate that his results may be more general and apply for the pure transition elements.

C. Results of Superconducting Attenuation in Nb[100]

In Figure 8, α_s/α_n for Nb[100] has been plotted with longitudinal waves of frequency 45.9 MHz. The background attenuation is approximately 5 percent of α_n for this crystal. Also given in Figure 8 are the BCS curves for the normal energy gap $A \equiv 2\Delta(0)/kT_c = 3.52$ and the BCS curve for an abnormal energy gap $A = 7.0$. The deviations of the experimental points from the normal BCS curve are very substantial. The initial reaction was to try to attribute the discrepancies between the experiment and the BCS theory to various possible apparatus problems. Some of these attempts are discussed in Appendix C. No way was found to explain these discrepancies in terms of a faulty experiment. For the following reasons, it is believed that these data present an accurate picture of the behavior of high-purity Nb[100] ($\Gamma = 6500$):

1. S. Sekula, Private Communication, Oak Ridge National Laboratory.

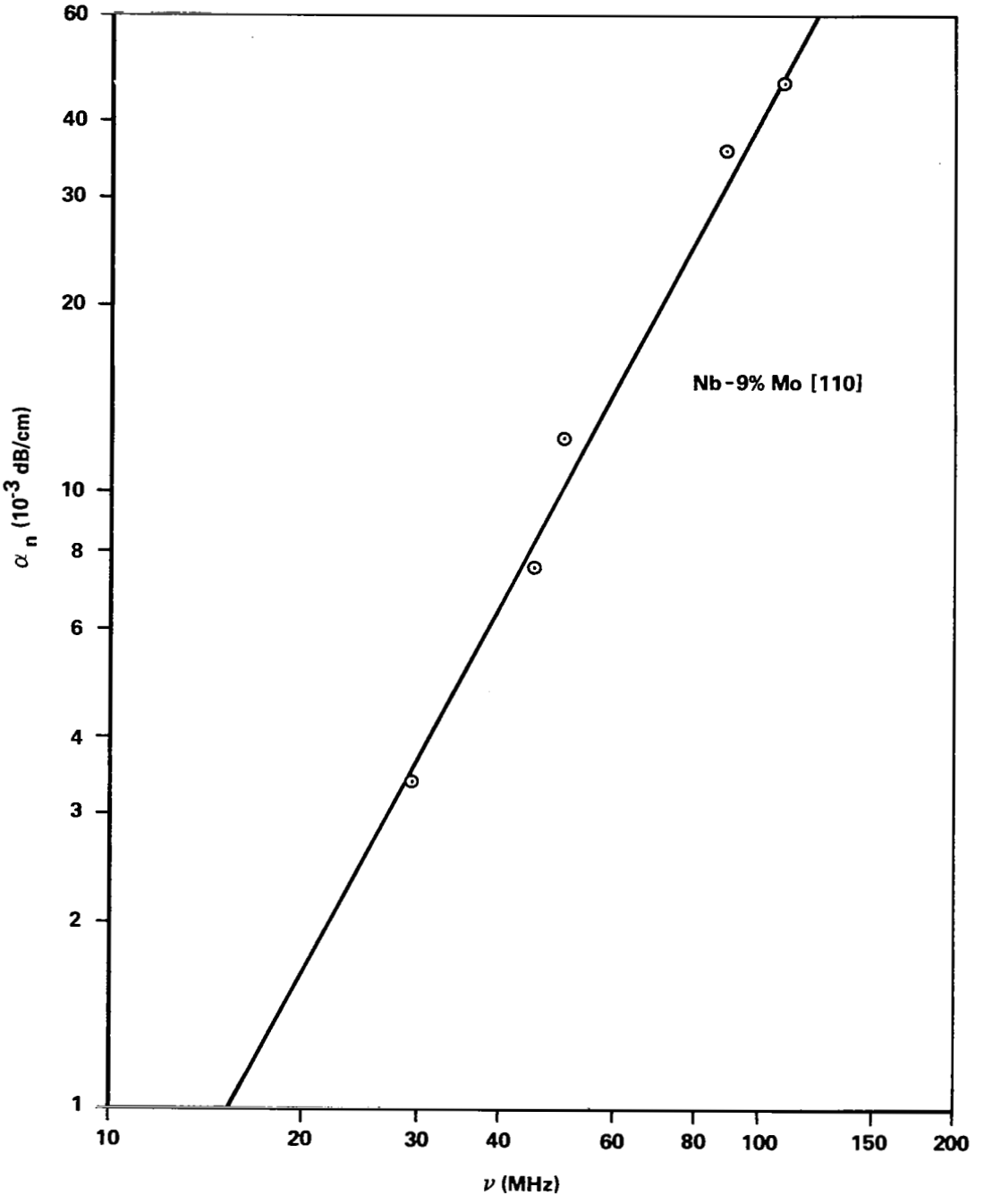

Figure 6. Normal Electron attenuation as a function of ultrasonic frequency.

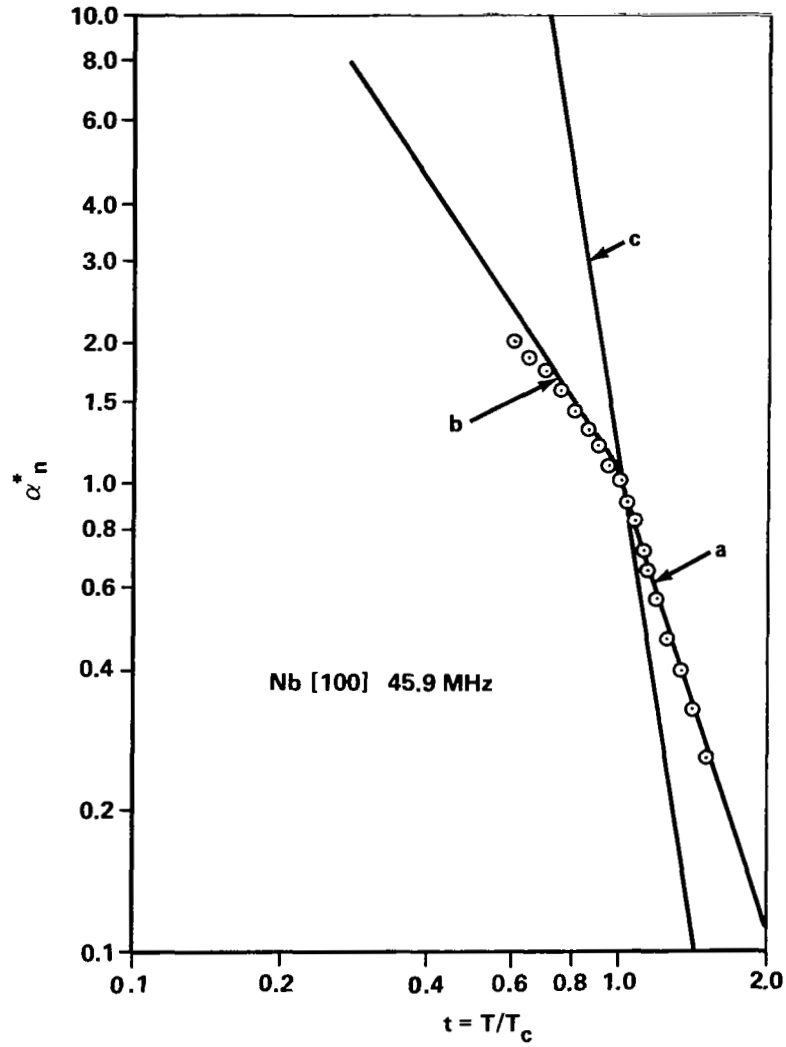

Figure 7. Reduced normal electron attenuation as a function of reduced temperature (The curves a and b are experimental whereas curve c shows Bloch's T^5 Law).

1. The results are reproducible with respect to increasing and decreasing temperature.

2. The data are reproducible with respect to measurements made on different echos. This would reveal any nonlinearity of the rf amplifier system.

3. The signal-to-noise ratio of the experiment is about 200.

4. The results are reproducible with respect to frequency (i.e., $q\ell_e$ varies from 0.1 to 1.3).

5. Figure 9 shows the resulting effective energy gap of the sample when equation (1) is solved for $\Delta(T)/kT_c$ using the data of Figure 8. The effective energy gap approaches the BCS value 3.5 as the temperature t approaches zero.

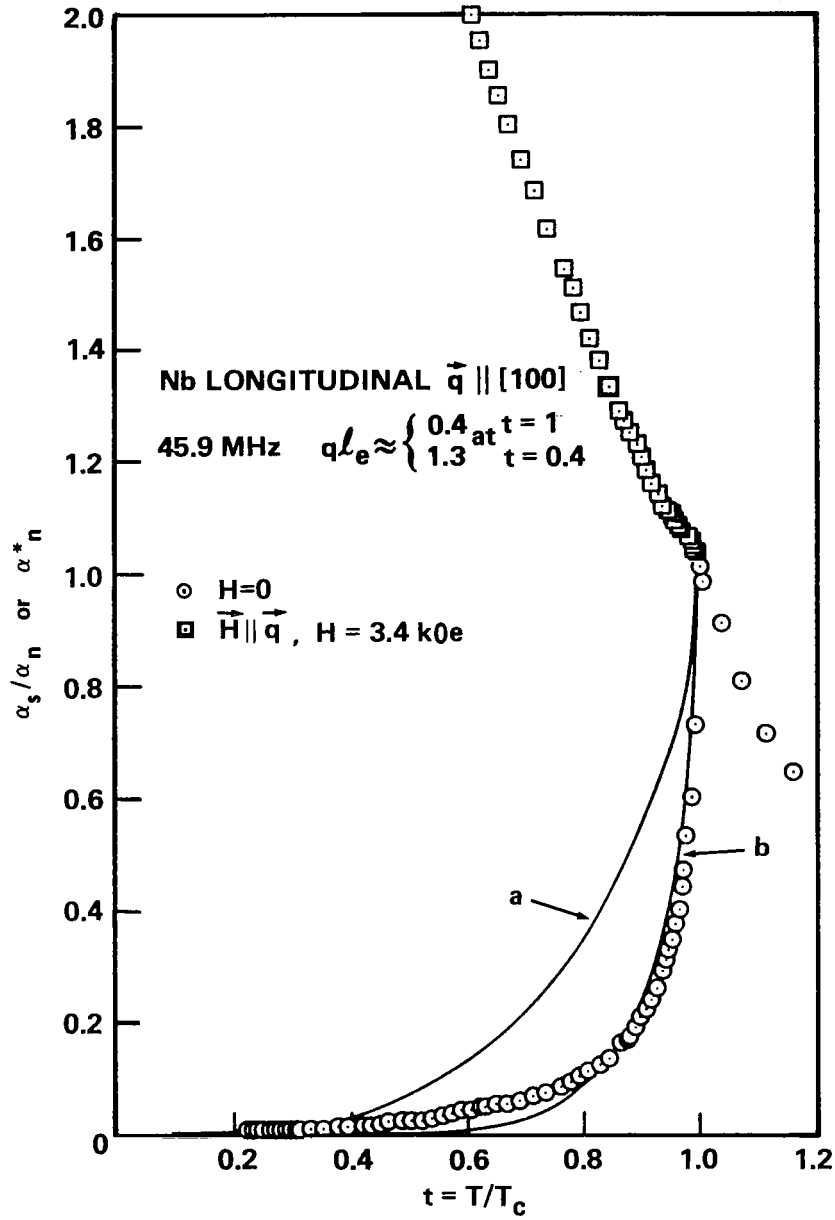

Figure 8. Superconducting and normal electron attenuation in Nb[100] (Curve a is the BCS theory for A = 3.53; curve b is the BCS type curve with A = 7.0).

6. Similar, although much less apparent, discrepancies have been obtained by several different experimenters using Nb, Pb, and Sn.

7. The effect can be explained simply by the assumption that Nb has two energy gaps.

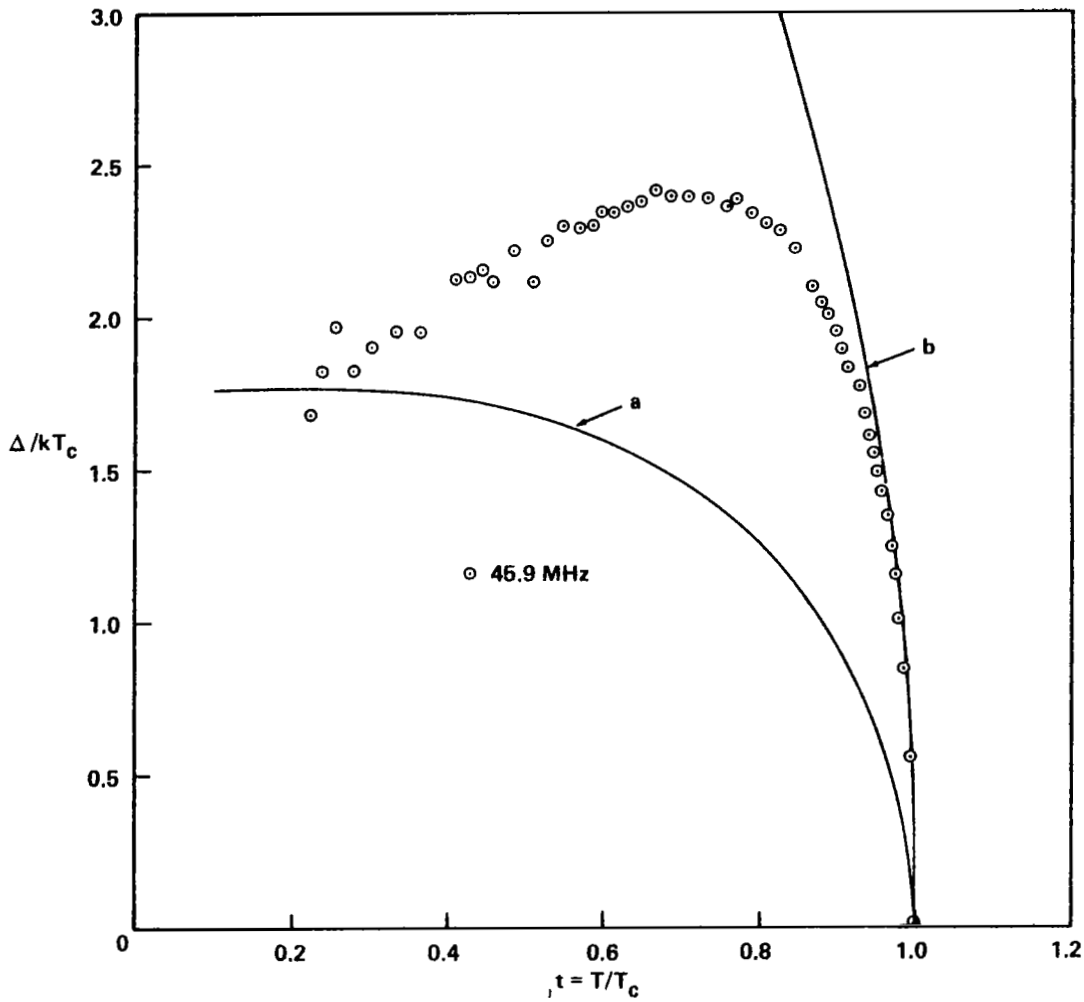

Figure 9. Effective energy gap in Nb[100] (Curve a is the BCS theory for A = 3.52; curve b is the BCS type curve with A = 9.0).

Items 5, 6, and 7 will be discussed separately. Two interesting observations may be made in Figures 8 and 9. The first is the previously mentioned fact that the gap approaches the BCS value for low temperatures. Other investigators have noted that if a material should have two gaps, the attenuation data will approach the smaller of the two gaps as the temperature approaches zero. This can be seen easily from the exponential behavior of the BCS attenuation equation at low temperatures. The second observation about the data on Nb[100] is that for $t \lesssim 1$ there is an extremely rapid decrease in the attenuation corresponding to a possibly anomalously large energy gap. The attenuation results of the Nb investigated here are very similar to those of Pb as noted by Deaton [21]. Claiborne [22] has also reported anomalously large gaps in Sn.

Both of the observations based on data of these experiments can be seen in the data of Perz [10] and Tsuda [11] taken from ultrasonic attenuation measurements on Nb. The major differences between the three sets of data are in the magnitude of the effect. In the Nb sample investigated, the deviations with respect to BCS are much more pronounced. It is believed, however, that the differences in the data can be explained in terms of the purity of the Nb samples used. Tsuda [12] has shown that ultrasonic attenuation in Nb has the usual BCS behavior for samples with $\Gamma \lesssim 200$ and an anomalous behavior for $\Gamma \gtrsim 400$. Tsuda also showed that the anomaly increased for a sample with $\Gamma \approx 800$. From Perz's normal state attenuation data, it is estimated that his samples had Γ's of about 400. In a more recent paper, Perz gives $\Gamma = 300$, although there is no way to tell if this is one of the original samples. As previously noted, Γ of our Nb sample was estimated to be 6500. Calculations by Garland [23] reveal that the energy gap anisotropy in the transition metals will be smeared out by the s-d scattering unless the metal has a purity $\Gamma \sim 10^4$. Therefore, based upon both experimental observation and theoretical calculations, it seems reasonable to attribute the discrepancies to the high purity of the Nb sample.

Following the suggestion of Claiborne [24], the Nb attenuation data were analyzed by assuming

$$\alpha_s/\alpha_n = \sum_i \frac{Ai}{\exp[\Delta i/kT]} \quad , \tag{3}$$

where the sum is over the various energy bands for the material. This was accomplished by plotting the log of α_s/α_n as a function of 1/T. If one assumes that

$$\alpha_s/\alpha_n = A \exp\,[-B(T)/kT] \quad , \tag{4}$$

in some temperature ranges, the slope of the curve at a given temperature would correspond to an effective energy gap $B(T) = \Delta(T)$.

It was found that the data could be described by three straight lines (i.e., B is constant for some given temperature range). These temperature ranges and corresponding values of B and $2\Delta/kT_c$ were the following:

1. $1 \leqslant t \leqslant 0.971$, $B = 23$ and $2\Delta/kT_c = 46$,

2. $0.962 \leqslant t \leqslant 0.893$, $B = 8.68$ and $2\Delta/kT_c = 17.3$,

3. $0.813 \leqslant t \leqslant 0.24$, $B = 1.65$ and $2\Delta/kT_c = 3.30$.

Except for the third case, this analysis is difficult to accept; one obvious objection is the astronomical value of $2\Delta/kT_c = 46$ for case 1. Another conceptual difficulty is the constant value for the effective energy gap B for the first two cases.

The above analysis does provide, however, a feeling of how rapidly the attenuation drops in the temperature range $t \geqslant 0.9$. It is tempting to try to analyze the region of the rapid drop in terms of the calculations of Bobetic [25] who used the BCS equations and calculated α_s/α_n for $\hbar\omega/\Delta_0 \geqslant 0.5$ (the normal BCS results apply for $\hbar\omega/\Delta_0 \ll 1$). In the present case, $\hbar\omega/\Delta_0 \approx 1 \times 10^{-4}$, and $\hbar\omega/\Delta$ will not be of the order of one until $t \gtrsim 0.999$. There is no reason, therefore, to consider that this anomalous drop in attenuation is due to ultrasonic phonon energies approaching the value of the energy gap.

D. Model for α_s/α_n in Pure Nb

Calculations by Garland [23] indicate that the clean state for the transition metals will be experimentally distinguishable from the dirty state by the presence of at least two partially decoupled energy gaps which are, in general, anisotropic. Since no microscopic theory of ultrasonic attenuation in pure two-band superconductors exists, a phenomenological theory which is based upon the conclusions of a microscopic theory will be proposed. The simplest assumption is that the attenuation may be expressed in the following form:

$$\alpha^* = \alpha_s/\alpha_n = F_1\alpha_1^* + (1 - F_1)\alpha_2^* \quad , \tag{5}$$

where

$$\alpha_i^* = 2/\{\exp[\Delta_i(T)/kT] + 1\} \quad , \tag{6}$$

$i = 1$ or 2, and F_1 is the fraction of the ultrasonic attenuation due to the electrons associated with Δ_1. As a boundary condition[2] for all $T < T_c$, F_1 must vanish when Δ_1 vanishes, and F_1 must be equal to unity when Δ_2 vanishes. With this in mind, the following equation was chosen for all temperatures below T_c:

$$F_1 = \Delta_1(T)/[\Delta_1(T) + \Delta_2(T)] \quad . \tag{7}$$

Now if one normalizes the energy gaps $\Delta_1^* \equiv \Delta_i(T)/\Delta_i(0)$, F_1 becomes

$$F_1 = \{1 + (\Delta_2^*/\Delta_1^*)[\Delta_2(0)/\Delta_1(0)]\}^{-1} \quad . \tag{8}$$

It seems reasonable to assume that the normalized energy gaps Δ_i^* follow the usual BCS behavior; therefore, $\Delta_1^* = \Delta_2^*$ if the two gaps have the same T_c. F_1 is now a constant, independent of temperature, and given by

$$F_1 = \{1 + A_2/A_1\}^{-1} \tag{9}$$

$$F_1 = A_1/(A_1 + A_2) \quad ,$$

where $A_i = 2\Delta_i(0)/kT_c$. If the gaps have two different T_c, equation (8) must be used where F_1 would be a function of temperature. The data from this study on Nb would suggest that only one T_c must be considered for pure Nb but that two different T_c must be considered for the Nb-Mo alloys.

Figure 10 shows an optimum fit of equations (5) and (9) to the data when $A_1 = 3.4$ and $A_2 = 10$. The value of A_1 is in reasonable agreement with the current microscopic theory, but the value of A_2 is difficult to understand even for strongly coupled superconductors, where $2\Delta(0)/kT_c = 4$. Figure 10 also shows that A_2 is independent of, or at least only weakly dependent on, $q\ell_e \approx 1$. The data in this report, combined with the data of Tsuda and Perz, suggest that A_2 is strongly dependent on the purity of the Nb sample (i.e., ℓ_e) as suggested by Garland's two-energy-band model.

2. This boundary condition only requires that equation (5) fit a BCS superconductor with a single energy gap.

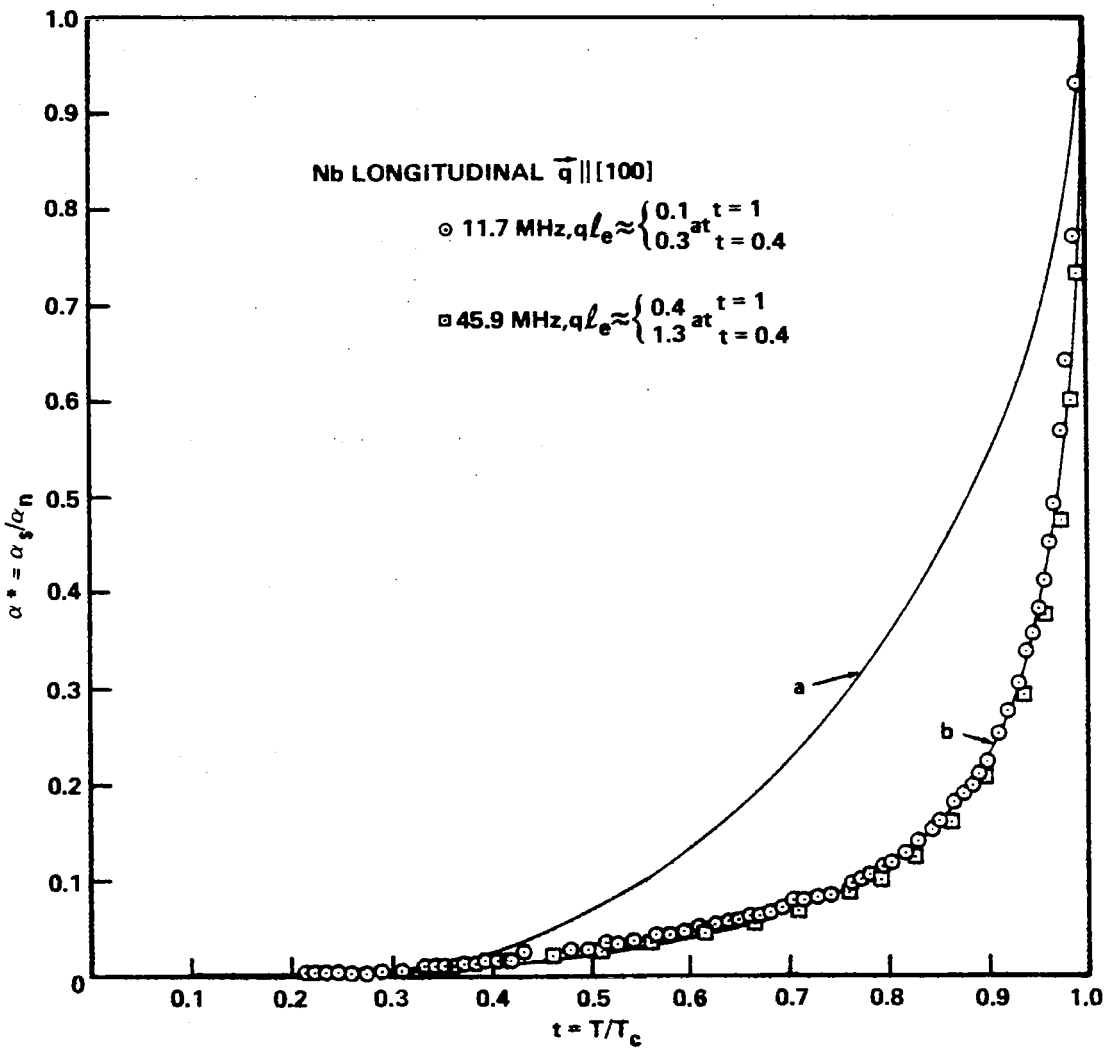

Figure 10. Superconducting attenuation in Nb[100] showing that the anomalous results are independent of $q\ell_e$. (Curve a is the BCS theory for A = 3.52; curve b is the two energy-gap model with $A_1 = 3.4$ and $A_2 = 10$).

Tsuda has shown that one energy gap was sufficient to fit his data over intermediate temperatures for Nb samples with $\Gamma \approx 200$ and that the anomalous results were obtained when $\Gamma \approx 400$. Tsuda's observations imply that the value of A_2 is reduced by impurity scattering which mixes the s and d energy bands (i.e., $A_2 \approx A_1 \approx 3.5$). When $A_2 \approx A_1$, equations (5) and (9) reduce to the usual BCS results for one energy gap. For $\Gamma \approx 400$, the energy gaps are apparently partially decoupled. The data of Perz and Tsuda would indicate that $A_2 \approx 5$ for $\Gamma \approx 400$.

The existence of a second partially decoupled energy gap in Nb for intermediate purities ($\Gamma \approx 400$) does not agree with the data of Weber [8], whose sample has a Γ of 500 and a single energy-gap value of 3.6. The discrepancy between the data of Tsuda and that of Weber could be resolved if Γ of Weber's sample were overestimated by a factor of two or three. Weber's constant normal-state attenuation α_n for all temperatures $T < 9^\circ K$ indicates that his sample was not as pure as initially indicated.

The model derived by this study satisfactorily fits the observed attenuation results for Nb over a wide range of purity ($10 < \Gamma < 10^4$) and at all temperatures, $T < T_c$, provided that A_2 is considered a function of purity. A similar approach has been used by Claiborne [22] in the ultrasonic study of superconducting Sn. In Claiborne's analysis, F_1 was treated as an adjustable parameter to fit his data. Likewise, Claiborne required large energy gaps ($A_2 \lessapprox 16$) to fit his data at intermediate temperatures.

E. Attenuation Results for Nb-Mo Alloys — Evidence for a Second Energy Gap in Nb-Mo Alloys

The ultrasonic measurements on the pure Nb sample were for $q\ell_e \approx 1$. All ultrasonic measurements on Nb-Mo alloys will have $q\ell_e \ll 1$ due to the limiting of ℓ_e by impurity (i.e., Mo) scattering. As discussed in Section I, the BCS resu'ts for α_s/α_n should still apply.

The experimental attenuation data for Nb-9%Mo[100] are given in Figure 11, where the error bars represent the total estimated uncertainty. The background attenuation for the Nb-Mo crystals are approximately a factor of 10 greater than α_n. A BCS curve for A = 4.2 has also been plotted. The experimental points deviate significantly from the BCS type curve in two different temperature regions $t \leqslant 0.65$ and $t > 0.92$. The effective energy gap calculated from the data and presented in Figure 12 also shows large deviations from the BCS theory.

The deviations for $t > 0.92$ can be explained in terms of a concentration gradient of Mo over the length of the Nb-9%Mo crystal. The measured midpoint of the transition temperature curve of this crystal is $T_c = 7.01 \pm 0.02$ K; the transition temperature curve has a width of $\Delta T_c = 0.28$ K. Many researchers of superconductivity define T_c as the temperature at which the sample is one-half superconducting and one-half normal as measured by the resistive technique. This study uses the same definition for T_c measurements using the inductive technique. Since T_c of Nb-Mo is known as a function of Mo concentration, ΔT_c can be used to calculate the concentration gradient of Mo. One then finds that $T_c = 7.0$ K corresponds to 9 atomic percent Mo, and $\Delta T_c = 0.28$ K corresponds to a variation of 1.1 percent Mo over the length of the sample. That is, the average concentration of Mo is 9 percent, but it varies from about 8.5 percent Mo at one end of the crystal to about 9.5 percent at the other end. These values are in reasonable agreement with an analysis furnished by the supplier who analyzed samples cut from the two end faces.

As previously mentioned, a linear concentration gradient of Mo can be used to understand the deviations of the α_s/α_n data for $t > 0.92$. The transition temperature of each part of the crystal will be given by

$$T_c = \frac{X}{L} \Delta T_c + T_{c0} \quad , \tag{10}$$

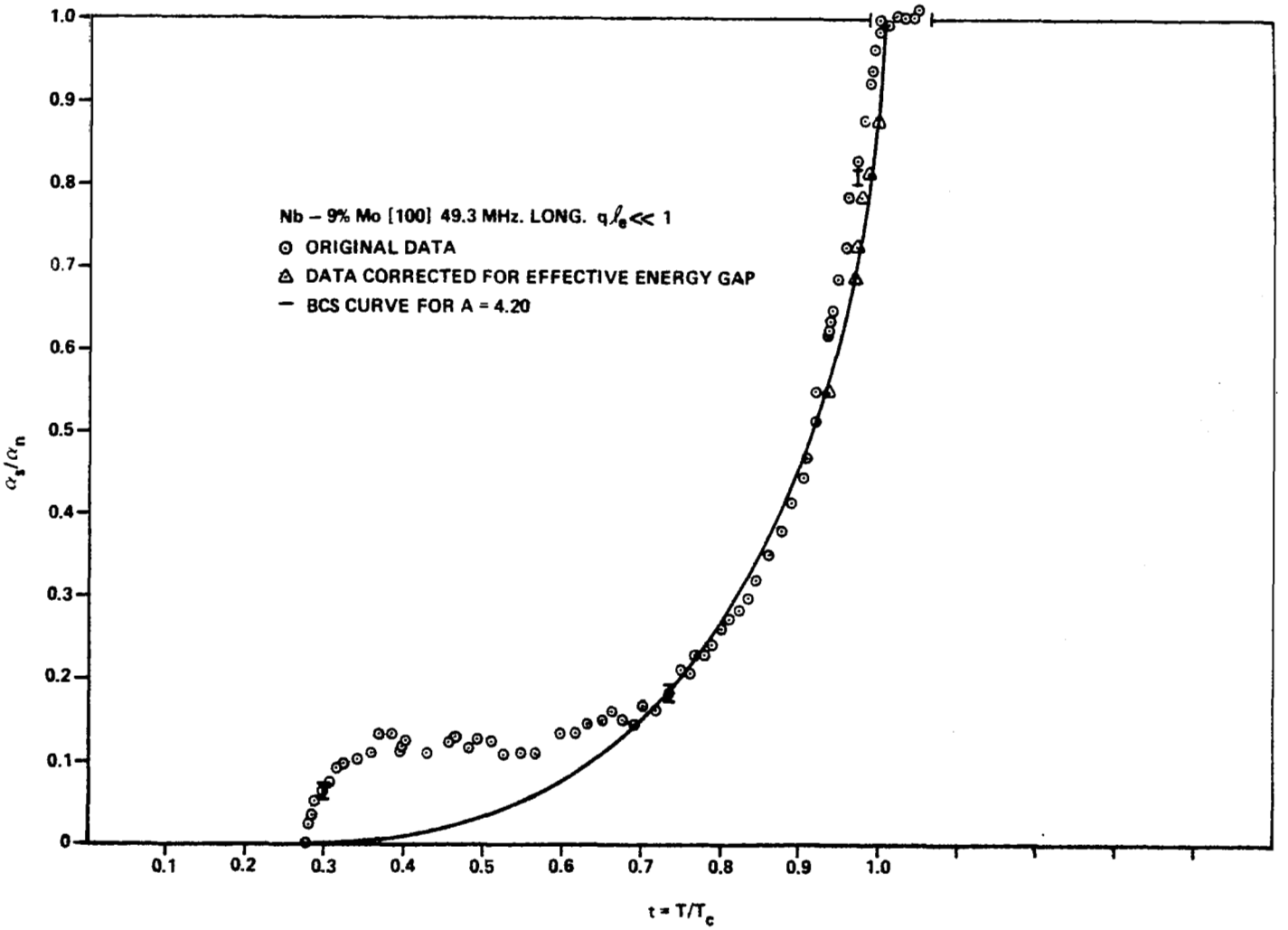

Figure 11. Superconducting attenuation in Nb-9%Mo[110].

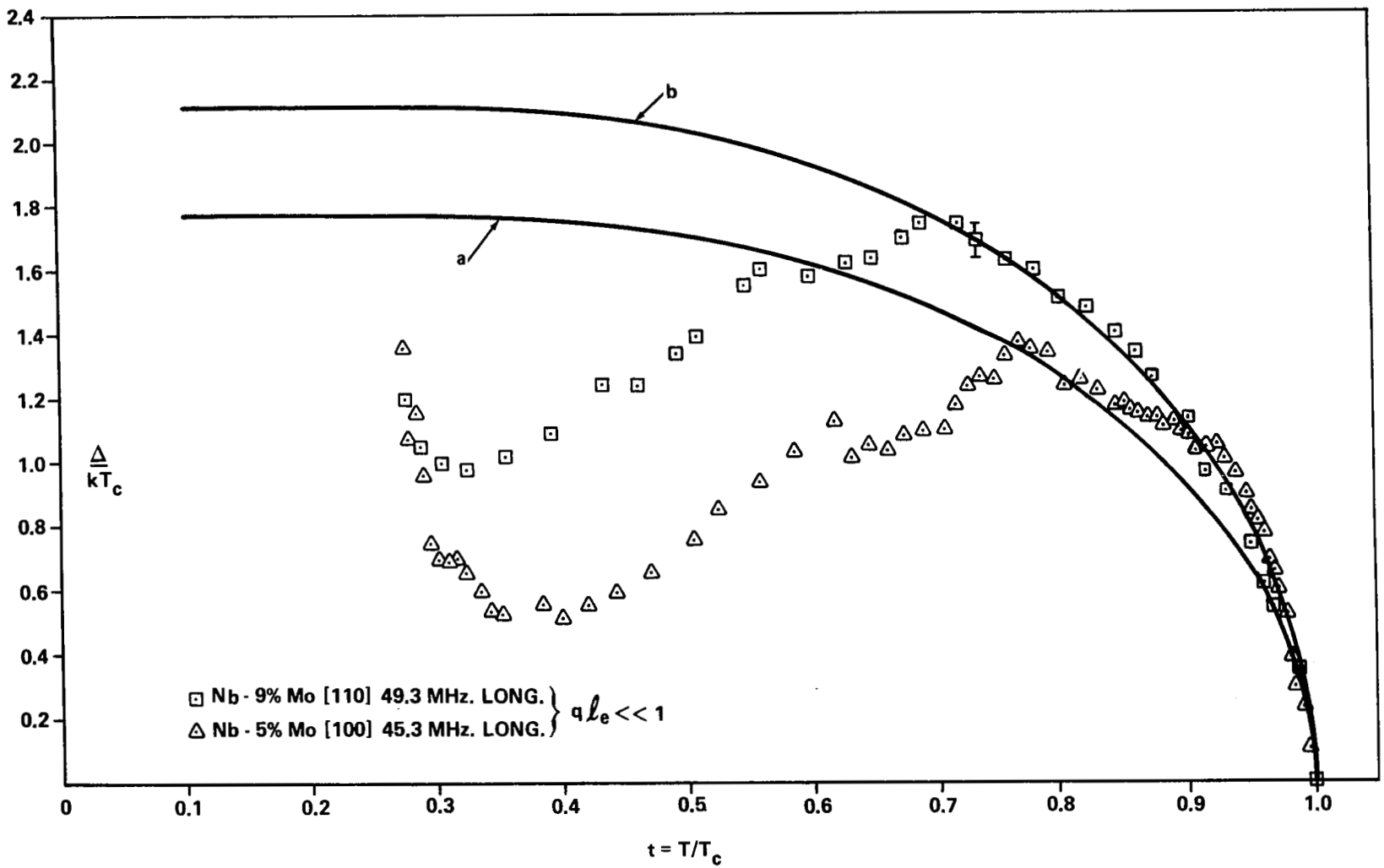

Figure 12. Effective energy gap for two Nb-Mo alloys (Curve a is the BCS theory for A = 3.52; curve b is the BCS theory for A = 4.2).

where T_{c0} is the lowest T_c corresponding to the highest Mo concentration, and X specifies a given location along the length of the sample. If one assumes for each part of the sample that $A \equiv 2\Delta/kT_c$ is a constant (for some given temperature), then Δ can be expressed in terms of the gradient of T_c:

$$\Delta(X) = A(X\Delta T_c/L + T_{c0})/2 \quad . \tag{11}$$

In an ultrasonic experiment, the sound wave will sample an average energy gap $<\Delta>$ along the length of the sample:

$$<\Delta> = \int_0^L \Delta(X)dx/L = A(\Delta T_c/2 + T_{c0})/2 \quad . \tag{12}$$

This is merely the definition of T_c as the half-point $T_{c½}$, and we conclude that

$$A = 2<\Delta>/kT_{c½} \quad . \tag{13}$$

Using this formulation, it is seen that for low temperature ($T << T_c$), the average gap $<\Delta>$, measured ultrasonically, and the real Δ for the material are essentially the same. For temperatures ($T \approx T_c$) were the gap Δ is small, the average gap $<\Delta>$ can deviate significantly from the gap Δ. In Figure 11, the original data (given by circles) have been corrected to the new values (given by triangles) to account for the average gap. The triangles give better agreement between theory and experiment with A = 4.2. This type of deviation of ultrasonic data has been observed by many of the early experimenters (1958-1964) for $T \approx T_c$ in "pure" samples. It now seems reasonable to attribute some of these earlier discrepancies to the rather impure "pure" materials available at that time.

The deviations from theory that have been observed for Nb-Mo alloys for $t < 0.7$ are still perplexing. It was originally thought that the deviation may be caused by some unusual occurrence in the experimental setup, such as changes in the bond between the crystal and transducer, the loss of tensile strength of the CuBe spring at low temperatures, or the loss of the system's vacuum at the liquid helium λ point. Additional experiments, however, ruled out these possibilities. The normal-state attenuation was measured to the lowest obtainable temperatures by placing the sample in a magnetic field, $H > H_{c2}$. As can be seen for Nb-5%Mo[100] in Figure 13, nothing unusual happens to the normal-state attenuation for $t \gtrsim 0.35$. The conclusion was that the rapid change in attenuation for $t \gtrsim 0.35$ is a superconducting property of the Nb-Mo alloy system which is roughly independent of Mo concentration and crystallographic direction.

The rapidity of the drop in attenuation for $t < 0.35$ and the lack of any "leveling out" of the drop for the lowest attainable temperatures gives evidence of another energy gap developing at t = 0.35. This could occur only if another phase of the material were present with a T_{c2} corresponding to 0.35 T_c of the Nb-Mo system. The zero of α_s/α_n at t = 0.28 can be misleading since α_s was arbitrarily defined as zero for the lowest obtainable temperature. This was necessary, since only measurements of the relative change in attenuation when the sample becomes superconducting were being made. Appendix A explains in more detail the method of analysing the attenuation data.

The idea of a second T_c in a "dirty" superconductor is not new. However, it has not been widely discussed previously due to the experimental difficulties of observing a second T_c in a material. Superconductivity is probably the only phenomenon studied in the laboratory which is a "perfect" state of matter. By

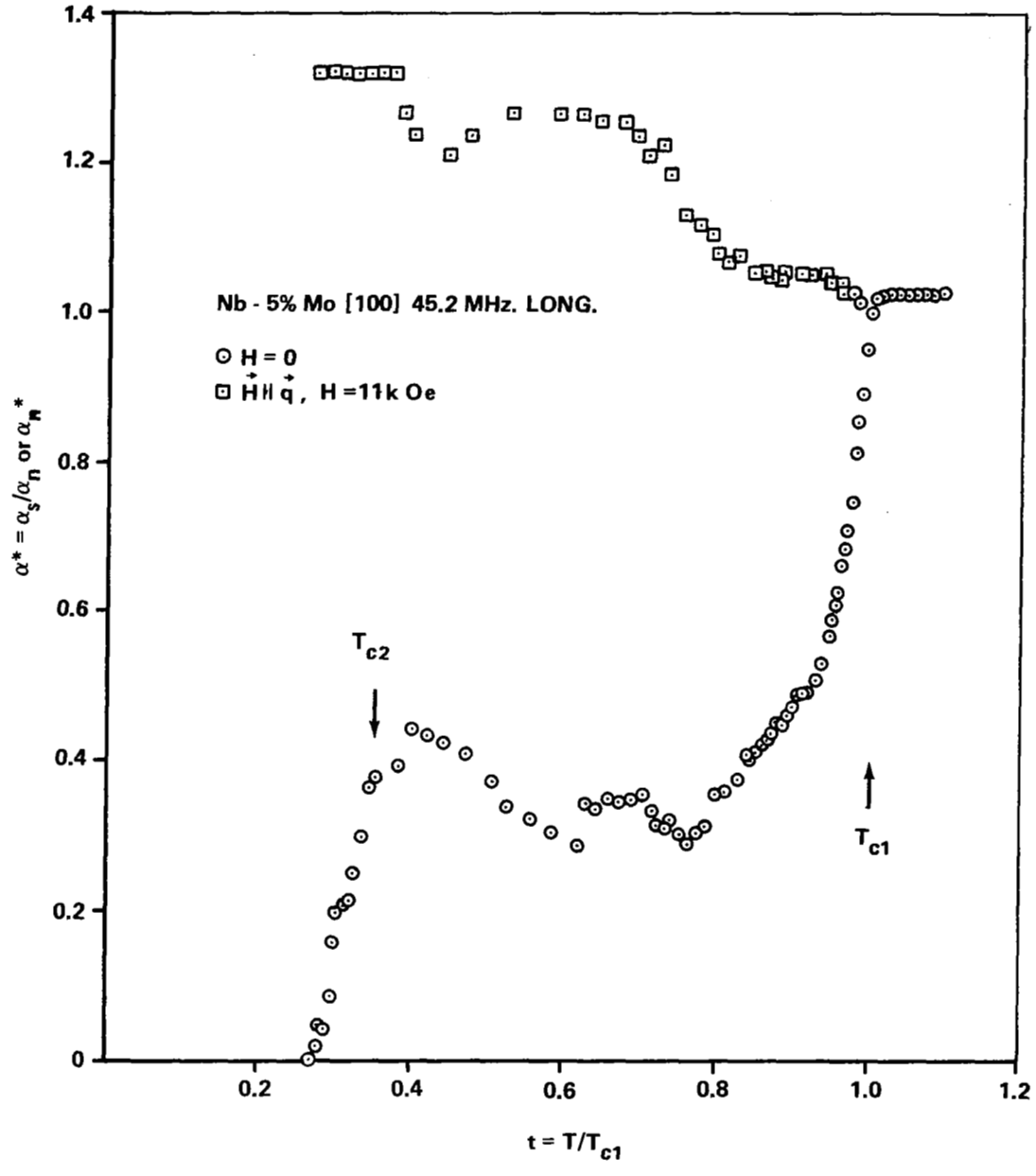

Figure 13. Superconducting and normal electron attenuation in Nb-5%Mo[100].

"perfect" one refers to the fact that the electrical resistivity of a superconductor is probably absolutely zero and not just nearly zero. This being the case, it is almost impossible experimentally to detect a second T_c in a material, since the material with the first and highest T_c shields our instruments from measuring any second T_c. This will be true for both resistivity and magnetic measurements. Matthias [26] and his coworkers recently have reported measuring a second phase in β-W materials such as Nb_3Sn, Nb_3Al, and V_3Si. His technique, however, involves destroying the sample by pulverizing and recompressing the powder to expose the maximum surface area for their magnetization measurements.

Unlike most of the other techniques for determining superconducting properties, ultrasonic techniques measure the average bulk properties of the superconductor. If Nb-Mo has a second phase, it seems reasonable that ultrasonic attenuation would detect this second phase.

Thus with the conclusion of a second T_c, $\alpha_s = 0$ at $t = 0.34$ was arbitrarily redefined, and the ratio of α_s/α_n for Nb-9%Mo was recalculated. The results are shown in Figure 14 and are in agreement with a theoretical BCS type curve with $A = 5.4$[3]. The agreement is good over the entire temperature range $0.34 \leqslant t \leqslant 1$ when account is also taken of the average energy gap for $t > 0.9$.

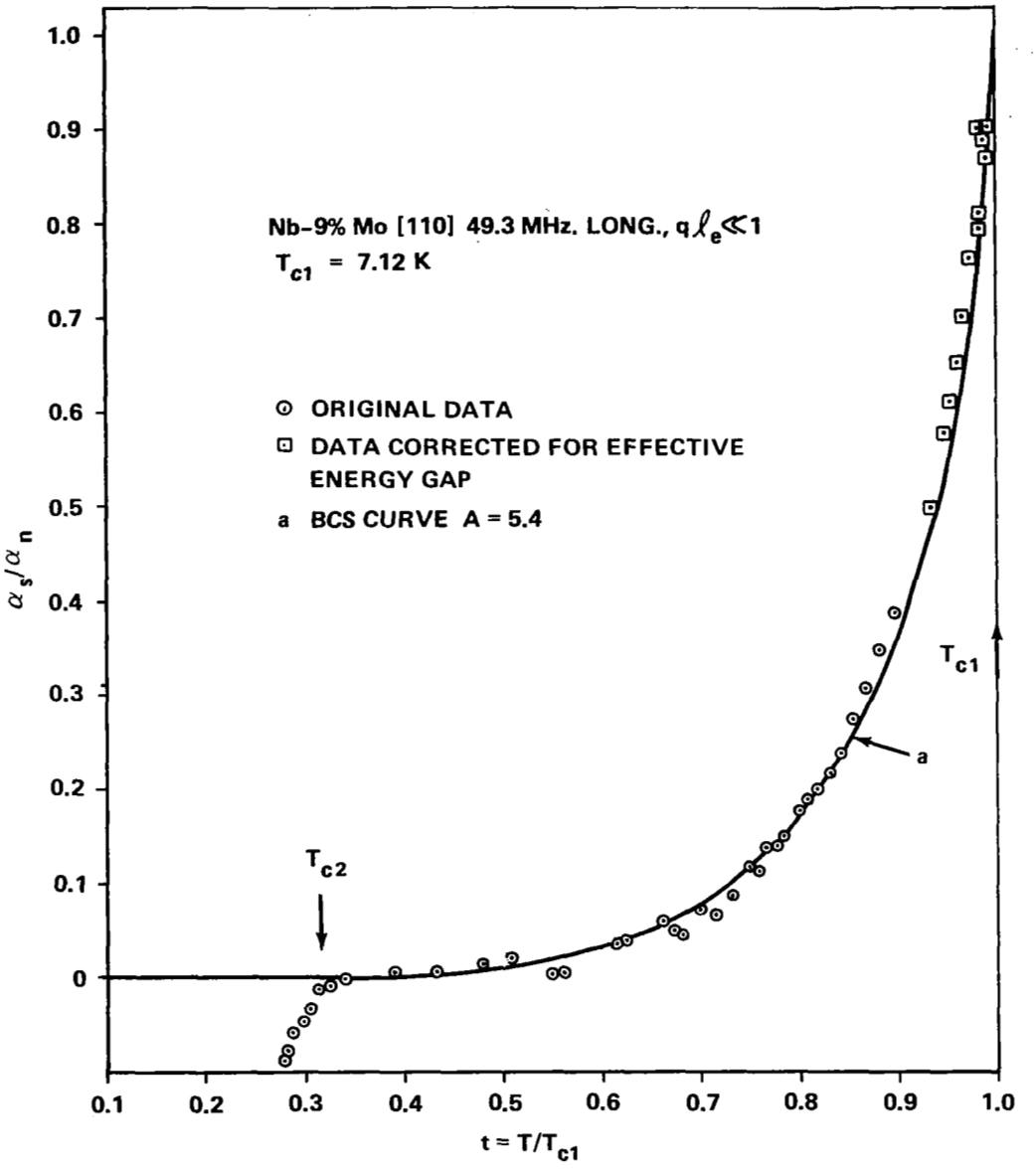

Figure 14. Superconducting attenuation in Nb-9%Mo[110] after defining T_{c2}.

3. The value of $A = 5.4$, implies that $\Delta(T = 0)$ for the alloy equals $\Delta(0)$ for impure Nb.

The same procedure is more difficult to apply to the Nb-5%Mo data; for unlike the Nb-9%Mo data, it is not clear where α_s should be set equal to zero. This difficulty arises due to the strange broad peaks at $t = 0.7$ and the even stranger increase in attenuation for $0.4 < t < 0.6$. For this reason, the Nb-5%No data were not analyzed in the above manner, although the same rapid drop in attenuation was observed for $t < 0.4$.

It is believed the main difference between the data for Nb-9%Mo and Nb-5%Mo can be understood in terms of annealing. The Nb-5%Mo is an unannealed sample, and Nb-9%Mo was annealed at 900°C in an atmosphere of 99.995 percent pure neon for one week. Claiborne [27] noted structure or absorption peaks in his attenuation data on polycrystals of Nb-1%Zr, Nb-2%Zr, and Nb-0.8%Mo. He attributed this to a density modulation of the electronic free energy and found that the behavior is strongly dependent on the strain and defect content of the sample. Claiborne has shown that the amplitudes of these oscillations are greatly reduced by annealing. Even in the annealed sample of Nb-9%Mo, the apparent scattering of the data for $0.35 < t < 0.7$ is probably caused by this effect. However, this is beyond the scope of this study except to note that before meaningful comparison can be made between the energy gaps in the Nb-Mo samples, the Nb-5%Mo should be annealed.

Additional support for the idea of a second phase in Nb-Mo can be found from the velocity data for "pure" Nb[110]. A small, but reproducible, transformation can be seen in the data at $t = 0.47$. That this "pure" sample contains a measurable amount of impurity which is probably Mo can be seen in the resistivity measurements made on these crystals at liquid nitrogen temperatures. Mo is usually the main impurity in commercial grades of Nb. Our measurements indicate that about 0.1 to 0.3 percent Mo may be found in the "pure" Nb[110] sample which has a measured $\Gamma = 74$.

Likewise, additional support for the idea of a second T_c in Nb-Mo is supplied by the small discontinuities seen in the attenuation data of Levy [7] on "pure" Nb[110]. Levy's sample had a measured resistivity ratio of 8 which is the same magnitude as for the Nb5%Mo studied here. The discontinuities occurred at $t \approx 0.32$ to 0.38. The rapid fall region in this experiment occurs at $t \approx 0.35$ for Nb-9%Mo and $t \approx 0.38$ for the Nb-5%Mo.

F. Summary of Attenuation Results

In summary, the results of these attenuation measurements on the Nb-Mo system are reviewed in Figure 15. Figure 15A illustrates the results of the two energy gaps with one T_c observed in pure Nb (curves a and b where $\Gamma \approx 6 \times 10^3$). In contrast to the recent theoretical prediction of Chow [28], there is no experimental evidence of a second different transition temperature associated with the second energy gap observed in pure Nb. Chow, however, did not take into account the possible mixing of the electron states due to thermal phonon scattering. The fact that electron scattering from thermal phonons is a dominate process in pure Nb is evident from the behavior of the normal electron attenuation α_n at low temperatures. The two energy gaps in Nb change to one energy gap for impure Nb (curve c where $\Gamma \approx 200$) as shown by Tsuda [12]. Only one gap is observed for impure Nb due to impurity scattering between the s and d energy bands as discussed by Garland [23].

For large concentrations of Mo (5 to 10 percent) where $\Gamma < 10$, Figure 15B shows that the one gap of Tsuda (curve c) goes over to two gaps (curves d and e) which have in this case two different transition temperatures, T_{c1} and T_{c2}. Curve f represents the energy gap for pure Mo. Intuitively, one would expect that curve d is associated with curve c when Mo is added to Nb and that curve e is associated with curve f

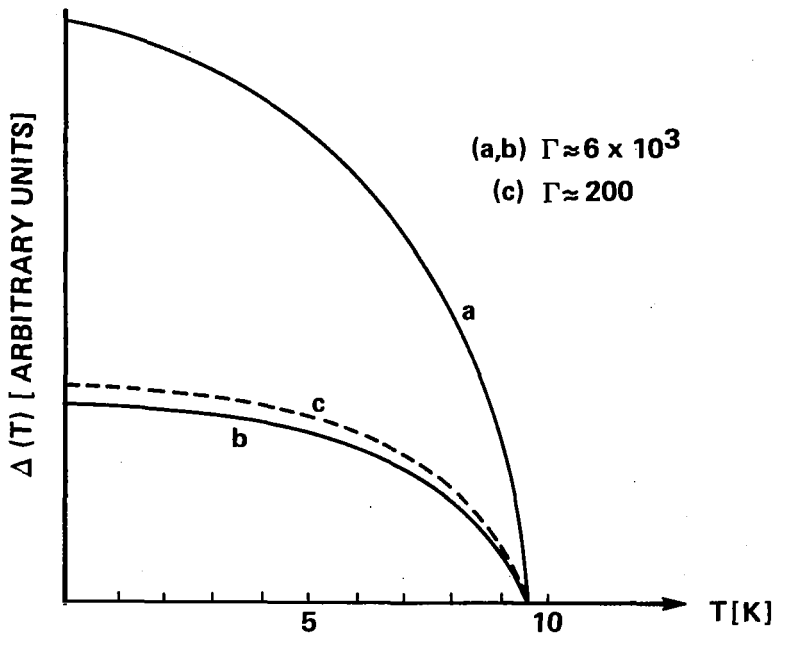

A. Nb

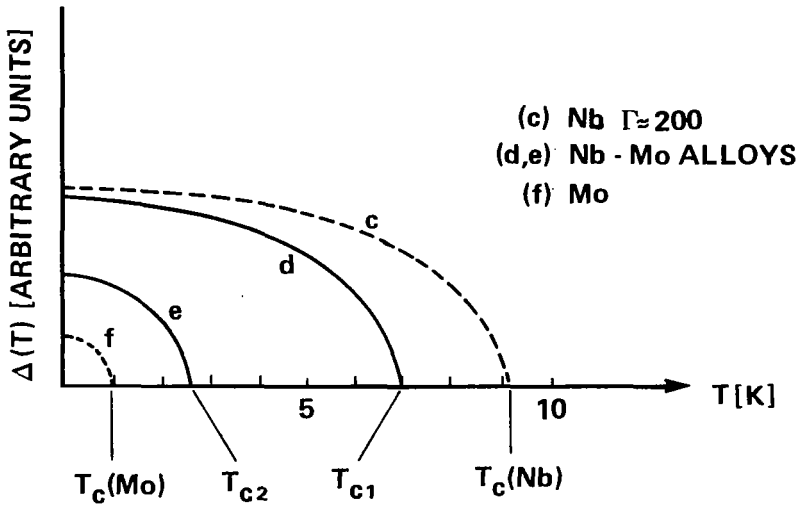

B. Nb-Mo Alloys

Figure 15. Energy gaps experimentally observed in Nb and Nb-Mo alloys as a function of temperature.

when Mo is enriched with Nb. Therefore, the idea of two energy gaps observed in Nb and Nb-Mo is not believed to be related. The second energy gap observed in Nb-Mo alloys is believed to be a second superconducting phase of the alloy associated with the energy gap of Mo when Mo is in a solid solution of Nb. Both of the energy gaps associated with curves d and e are uncertain since the attenuation experiments could not be performed at low enough temperatures.

SECTION III. VELOCITY MEASUREMENTS AND ELASTIC CONSTANTS

A. Absolute Velocity Measurements

The absolute ultrasonic velocity of each sample was found by measuring the transit time between a pair of echos. A schematic of the measuring system is shown in Figure 16. The central part of this experiment is the 5360A Computing Counter made by Hewlett-Packard. This counter is capable of measuring time intervals to an absolute accuracy of 1 ns and a relative accuracy of 0.1 ns. For a typical transit time of 10 μs, this allows an absolute measurement of transit time to an accuracy of 0.01 percent.

The above feature by itself would make this a very valuable measuring system. The computing counter has, however, an additional feature which greatly extends the sensitivity of the system for measuring small changes in the velocity of sound. By using the small computer of the computing counter, one can digitally average the transit time for 10 to 10 000 measurements, which effectively averages out the noise and jitter of our electronics and extends the measuring sensitivities of the system to 10 ps (i.e., 1 ppm change in the transit time). The technique described here represents the first time the same instrumentation was used to measure both the absolute velocity of sound and small changes in the velocity of sound.

Before proceeding with a description of the measurement, it is convenient to define the following experimental parameters:

τ_{12} measured transit time between echos 1 and 2,

τ_{in} measured transit time between echos i and n,

τ_0 true transit time, $\equiv 2L/v_s$,

Δt uncertainty in measured transit time, $\tau_0 - \tau_{in}$,

t_r risetime of an echo,

V_n the peak voltage of echo n, and

V_{tn} the trigger voltage for echo n.

With these definitions it is a simple matter of geometry to relate Δt to the various voltages. For triangular echos and a constant risetime, t_r, the uncertainty in the measured transit time, Δt, between echo n and n + 1 is given by

$$\Delta t = \frac{V_{tn+1}}{V_{n+1}} \left(1 - \frac{V_{tn}/V_{tn+1}}{V_n/V_{n+1}} \right) t_r \ . \qquad (14)$$

From equation (14) it can be seen that Δt vanishes if the ratio of the trigger voltages can be set equal to the ratio of the echo voltages. Likewise, Δt becomes small if the risetime t_r becomes small. In this system the trigger voltages can be measured accurately with a digital voltmeter (0.01 percent). The only

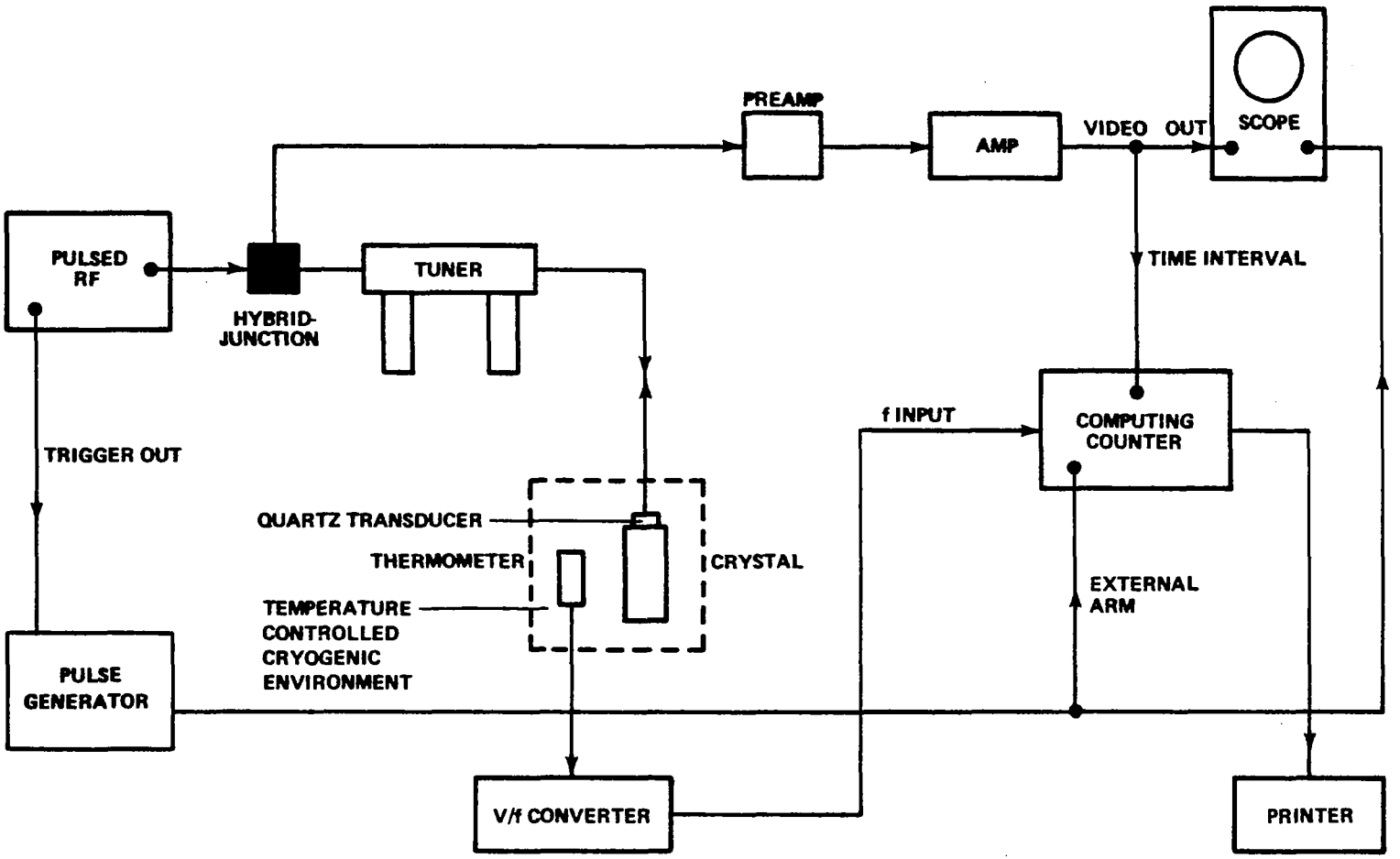

Figure 16. Schematic for ultrasonic velocity experiment.

uncertainty associated with the trigger voltages is the basic uncertainty associated with a Schmidt trigger (0.3 percent). The largest system uncertainty, however, is that associated with measurement of the various echo voltages (1 percent).

The following numerical example will give a better understanding of the magnitude of Δt. If one assumes

$$V_{tn}/V_{tn+1} \approx 1.01\ (V_n/V_{n+1}) \quad ,$$

$$V_{tn}/V_n \approx 0.10 \quad ,$$

$$t_r \approx 500\ \text{ns} \quad ,$$

$$\nu \approx 50\ \text{MHz} \quad ,$$

and

$$\tau_{n,n+1} \approx 10\,\mu\text{s} \quad ,$$

then $\Delta t \approx 0.5$ ns $\approx 5 \times 10^{-3}$ percent. Later it will be shown that this accuracy has not been achieved but that the absolute accuracy is 0.2 percent.

For a typical experiment, the measurements are made when the sample is at liquid helium temperatures. Transit times $\tau_{12}, \tau_{13}, \ldots \tau_{n-1,n}$ and $\tau_{13}, \tau_{14} \ldots \tau_{1n}$ are measured under two conditions : (1) The amplifiers are saturated to decrease t_r and V_{tn}/V_n and (2) With unsaturated amplifiers and exponential decay patterns, the average ratio $\left\langle V_{n+1}/V_n \right\rangle$ is measured on an oscilloscope and V_{tn+1}/V_t is adjusted to equal the average $\left\langle V_{n+1}/V_n \right\rangle$. The results for Nb-5%Mo with 45 MHz longitudinal waves in the [100] direction are given in Table 1.

It should be pointed out that each τ_{in} is a reproducible measurement within ±1 ns, and, from the above consideration, the absolute uncertainty in transit time for each measurement in approximately 1 ns. Each column in Table 1 has been averaged and the standard deviation is given. Also included in each column is the difference between the measured transit time for the given echo combination and the average transit time considering all echos.

From the standard deviations, it is immediately obvious that the measured uncertainties are a factor of 10 to 20 times the uncertainties of each measurement. Indeed, note that each technique reproduces the transit time to within $\Delta t \simeq \left(\frac{1}{\nu}\right) \simeq 20$ ns. At the present time, the measured uncertainties are larger than the capabilities of the instrumentation, and the measured uncertainties are always of the order of or less than one wavelength.

Another curious fact about this experiment is that the standard deviations of Column Three are always greater than the standard deviations of Column Seven. It is also interesting to note that the deviations in Column Seven seem to vary in a systematic way; whereas, the deviations in Column Three seem to be more or less random.

TABLE 1. MEASURED TRANSIT TIMES FOR Nb-5%Mo [100] 46 MHz LONGITUDINAL (4.2°K)

Echo Number (n–m)	τ_{nm}[a] (μs)	$\Delta\tau$ (ns)	Echo Number (n–m)	τ_{nm}[a] (μs)	$\tau_{nm}/(n-m)$ (μs)	$\Delta\tau$ (ns)
1–2	7.591	–24	1–3	15.205	7.6025	–14.3
2–3	7.611	– 4	1–4	22.824	7.6080	–18.8
3–4	7.614	– 1	1–5	30.476	7.6190	2.2
4–5	7.647	32	1–6	38.107	7.6203	4.6
5–6	7.624	9	1–7	45.722	7.6203	3.5
6–7	7.607	– 8	1–8	53.329	7.6184	1.6
7–8	7.602	–13	1–9	60.964	7.6205	3.7
8–9	7.628	13	1–10	68.585	7.6206	3.8
9–10	7.611	– 4	1–11	76.205	7.6205	3.7
10–11	7.611	– 4				
11–12	7.624	9	Avg		7.6168	± 6.8
Avg	7.615	±15				

a. All values are averages of 1000 digital measurements with saturated amplifiers.

Although the velocity measurements are limited in absolute value to a fraction of the ultrasonic wavelength, the experiment is still accurate enough to allow for a relative measurement of the phase shift of sound as it is reflected from the surface of the crystal. The two phase shifts, τ_{pb} and τ_{pt} are defined as the time corresponding to a phase shift of the sound for reflection from the back face of the crystal and the time corresponding to a phase shift of the sound for reflection from the surface of the crystal containing the transducer, respectively. If the faces of the crystal were perfectly hard and not in acoustical contact with other materials, then elementary wave theory would predict a 180-degree phase shift ($\approx$ 10 ns for 50 MHz waves). Let us assume that

$$\tau_{12} = \tau_0 + \tau_{pb} \quad , \tag{15}$$

or, in general

$$\tau_{n,\,n+1} = \tau_0 + \tau_{pb} \quad . \tag{16}$$

But τ_{13} must contain an additional term due to the phase shift at the transducer τ_{pt}; that is,

$$\tau_{13} = 2\tau_0 + 2\tau_{pb} + \tau_{pt} \quad , \tag{17}$$

and likewise

$$\tau_{1n} = 3\tau_0 + 3\tau_{pb} + 2\tau_{pt} \tag{18}$$

or, in general,

$$\tau_{1n} = (n-1)\,\tau_0 + (n-1)\,\tau_{pb} + (n-2)\,\tau_{pt} \quad . \tag{19}$$

Combining equations (16) and (19), one finds

$$\tau_{1n} - (\tau_{12} + \tau_{23} + \cdots\cdots \tau_{n-1,\,n}) = (n-2)\,\tau_{pt} \quad . \tag{20}$$

The data from Table 1, have been plotted in Figure 17 in accordance with equation (20). The slope of the straight line is τ_{pt} which is approximately 6.1 ns/echo or 0.28 $\left(\frac{1}{\nu}\right)$ /echo. The intercept of the straight line is n $\approx$ 2.5 and is in reasonable agreement with equation (20). The data for Nb-9%Mo [110] at ν = 11.1 MHz are also plotted in Figure 14. For Nb-9%Mo, the slope is 18 ns/echo or 0.20 $\left(\frac{1}{\nu}\right)$ /echo and the intercept is n = 2.2. It may be concluded, therefore, that the waves undergo about one-quarter-wavelength shift upon reflection from the crystal face containing the transducer.

B. Elastic Constants

The longitudinal and two transverse velocities of sound were measured for Nb[110] and and Nb-9%Mo[110] at 4.2°K. Then, the velocities were used to calculate the elastic constants of the material by using the equations derived by Truell [18]:

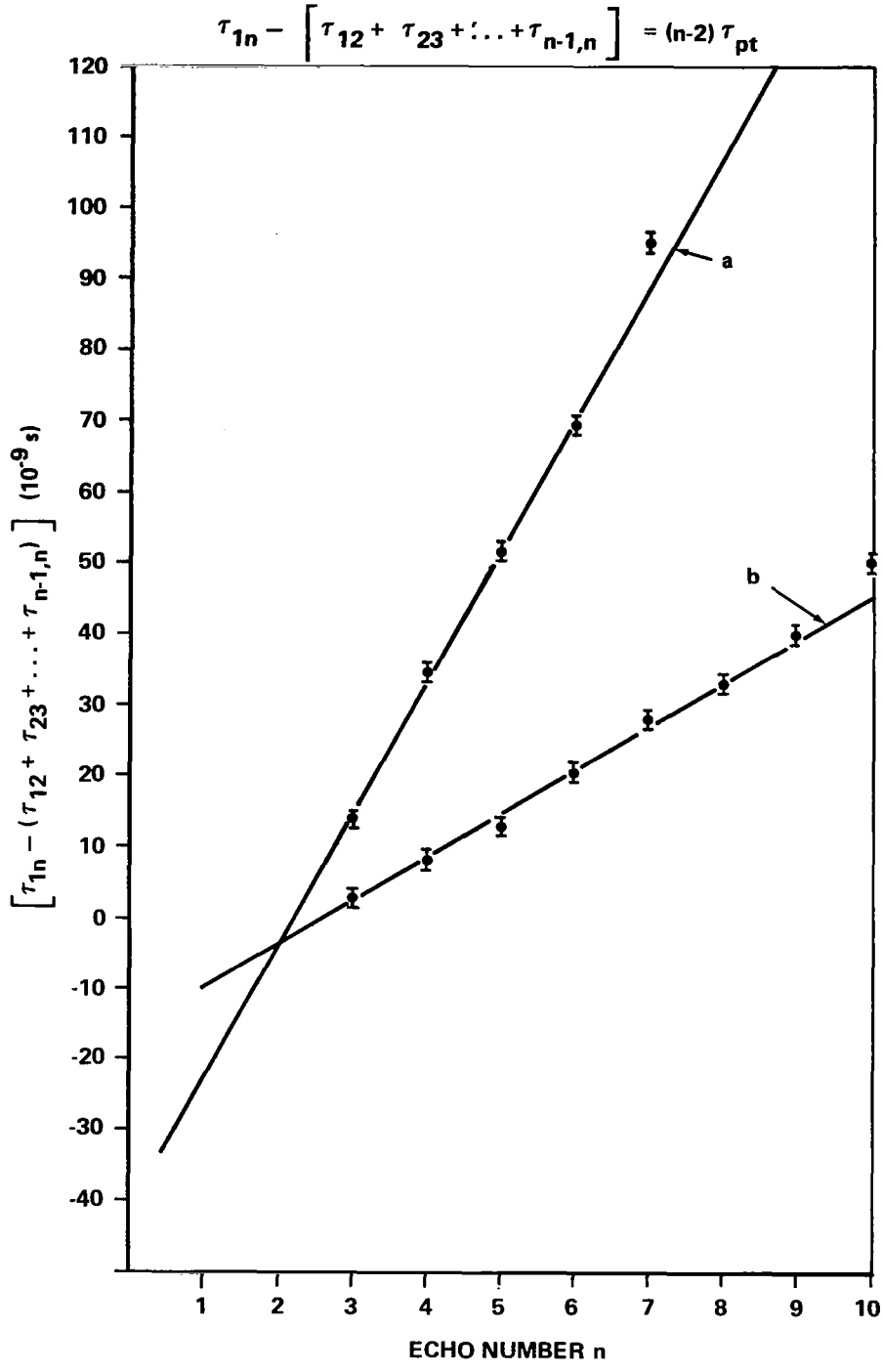

Figure 17. Method for measuring the phase shift at the transducer-sample interface τ_{pt} (Curve a is Nb-9%Mo[110] 11 MHz, 77°K; Curve b is Nb-5%Mo[100] 46 MHz, 4.2°K).

$$\rho V_{L2}^2 = (C_{11} + C_{12} + 2C_{44})/2 \ ,$$

$$\rho V_{T1}^2 = C_{44}, \text{ polarization in } [001] \ , \qquad (21)$$

$$\rho V_{T2}^2 = (C_{11} - C_{12})/2, \text{ polarization in } [1\bar{1}0] \ .$$

The velocity of sound was also measured for longitudinal waves in Nb-5%Mo and Nb along the [100] direction. These results are presented in Table 2.

The surprising conclusion to be drawn from these measurements is that the elastic constants of Nb-Mo are almost completely insensitive to the concentration of Mo for frequencies $\nu \lesssim 50$ MHz and concentrations of Mo to 9 atomic percent. If C_{11} is plotted as a function of Mo concentration, it varies linearly with concentration with a slope of 0.35 percent change in C_{11} per atomic percent of Mo. The elastic constants of Nb are so nearly constant that it is difficult in ultrasonic velocity experiments to tell the difference between pure Nb and Nb-5%Mo.

These results should be compared with the drastic changes in the superconducting properties of Nb when Mo is added to the material. It is found experimentally that the transition temperature T_c of Nb decreases linearly with the concentration of Mo with a slope of three percent per atomic percent of Mo. Indeed, Mo has 10 times the effect on T_c of Nb as on the elastic constants.

Using the elastic constants of Nb[110] and Nb-9%Mo, the Debye temperature θ_{De} was calculated using the Tedorov method given by Konti [29]. Here one finds $\theta_{De} = 275 \pm 1$ K for pure Nb compared with $\theta_{Dt} = 275$ K for the latest experimental thermal values given by Veal [30]. This agreement seems more than just fortunate, since Konti obtained good agreement between θ_{De} and θ_{Dt} for a large group of cubic elements. Using the same technique on Nb-9%Mo, the Debye temperature was found to be $\theta_{De} = 277 \pm 2$ K. If one uses the linear extrapolation given by Veal [30], $\theta_{Dt} = 297$ K. This 7 percent discrepancy is surprising considering the excellent agreement for the pure materials.

The discrepancy between θ_{Dt} and θ_{De} for Nb-9%Mo can probably be understood in terms of the basic assumptions made in the theory relating C_{ij} and θ_{Dt}. The measurements of C_{ij} are for frequencies $\nu \approx 10^7 - 10^8$ Hz and the theory assumes no phonon dispersion over the entire frequency range to $\Omega_D \approx 10^{13}$ Hz. Phonon dispersion for $\nu \approx 10^{12}$ Hz is evident from the dispersion curve of Nb given by Baz [31]. Therefore, if there is a difference between C_{ij} for Nb and C_{ij} for Nb-9%Mo, it would be expected to occur in the range $\nu \geqslant 10^{12}$ Hz. This may be understood by assuming that C_{ij} for Nb-9%Mo will remain fairly constant until the measuring wavelength is of the order of the distance between the Mo atoms. This would correspond to a frequency $\nu = 5 \times 10^{12}$ Hz.

As a final remark on the constant C_{ij} of Nb-Mo, it is interesting to note the theoretical work of Hopfield [14] who extended McMillan's theory [13] on T_c of elements and alloys by noting that the T_c of transition element alloys is limited by the elastic properties of the material. The measurements made for this report indicate that no significant correlations exist between the elastic properties and T_c of the Nb-Mo alloys for ultrasonic frequencies to 50 MHz.

TABLE 2. ELASTIC CONSTANTS OF Nb AND Nb-9%Mo

Sample	C_{11}[a] (10^{12} dynes/cm^2)	C_{12}[a] (10^{12} dynes/cm^2)	C_{44}[a] (10^{12} dynes/cm^2)	Temperature (°K)	Density (gm/cm^3)
Nb[110]	2.503	1.292	0.2940	77	-
Nb[110]	2.516	1.291	0.2989	4.2	8.6420
Nb[b]	2.527	1.332	0.3097	4.2	8.5715
Nb-9%Mo[110]	2.603	1.328	0.3010	4.2	8.7627

a. Estimated absolute accuracy ± 1 percent.
b. K. J. Carrol, J. Appl. Phys., No. 36, 1965, p. 3689.

C. Small Velocity Changes Associated with Superconducting Properties of Nb-Mo Alloys

The technique for measuring small ultrasonic velocity changes is essentially the same as for measuring the absolute velocity. The measuring system is triggered by two different echos (typically echos 1 and 10), and the measurements are averaged about 1000 times. For a typical pulse repetition frequency of 1 ms, a response time of 1 s is given for the instrumentation.

The computing counter is also used to measure the temperature of the sample. Figure 16 shows the electronic configuration. The voltage of the germanium thermometer is converted to a frequency by a voltage-to-frequency converter, and the frequency is read and printed by the computing counter. The computing counter then takes about 1000 measurements of transit time, averages the data, and prints the answer. The entire process is under the control of the computer. The data reported here were taken in a slightly different fashion, since the logic for the print circuit was not completed at the time of the experiment. The computing counter was used to measure the transit times, but a digital voltmeter was needed to measure the thermometer voltage.

Figure 18 represents the data for longtiudinal waves at 50 MHz for Nb[110]. The ordinate represents the fractional change in transit time $\Delta\tau/\tau$ in parts per thousand (0.1 percent). From the data, it is evident that a total sensitivity of 20 ppm (2×10^{-5}) has been achieved. The total change in transit time for T = 4.2 K to $T = T_c$ was 30.6 ns. The heating rate for the sample was about 1.6 mK/s which corresponds to 1.6 mK per response time for the instrumentation. It is interesting to note that there is a rapid change in velocity of 360 ppm within 20 mK of T_c.

The results for longitudinal sound waves in Nb-9%Mo[110] are presented in Figure 19. In this case, the ordinate represents the fractional change in velocity, $\Delta v/v$ in ppm (note $\Delta v/v = -\Delta\tau/\tau$). In this case the instrumentation has achieved a sensitivity of 1 ppm which rivals that of the sing-around method, the only other technique to achieve such sensitivities.

Little importance should be attached to the discontinuities which occur between 4 and 5 K. They are caused by liquid helium flowing onto the crystal and the transducer. The first and largest discontinuity (T = 4.7 K) is probably caused by the change in the phase shift as liquid helium flows over the bottom-end face of the crystal. From the magnitude of the effect (20 ppm), it can be calculated that the sound wave penetrated an additional 0.1λ at the liquid helium crystal interface. The other discontinuities are caused by the liquid helium flowing over the transducer and bond. This dramatically presents the reason for the later use of an evacuated system.

At the present time, there is no theory which attempts to relate changes in the elastic behavior between the superconducting and normal states. The results can be compared only with the free electron model of normal electrons developed by Steinberg [32].

For longitudinal waves with $q\ell_e \ll 1$, Steinberg obtains

$$v_s = v_0 \left[1 + \frac{3\alpha_n^2}{4q^2} \left(1 + \frac{5Mv_0^2}{mv_F^2}\right)\right]^{1/2}, \qquad (22)$$

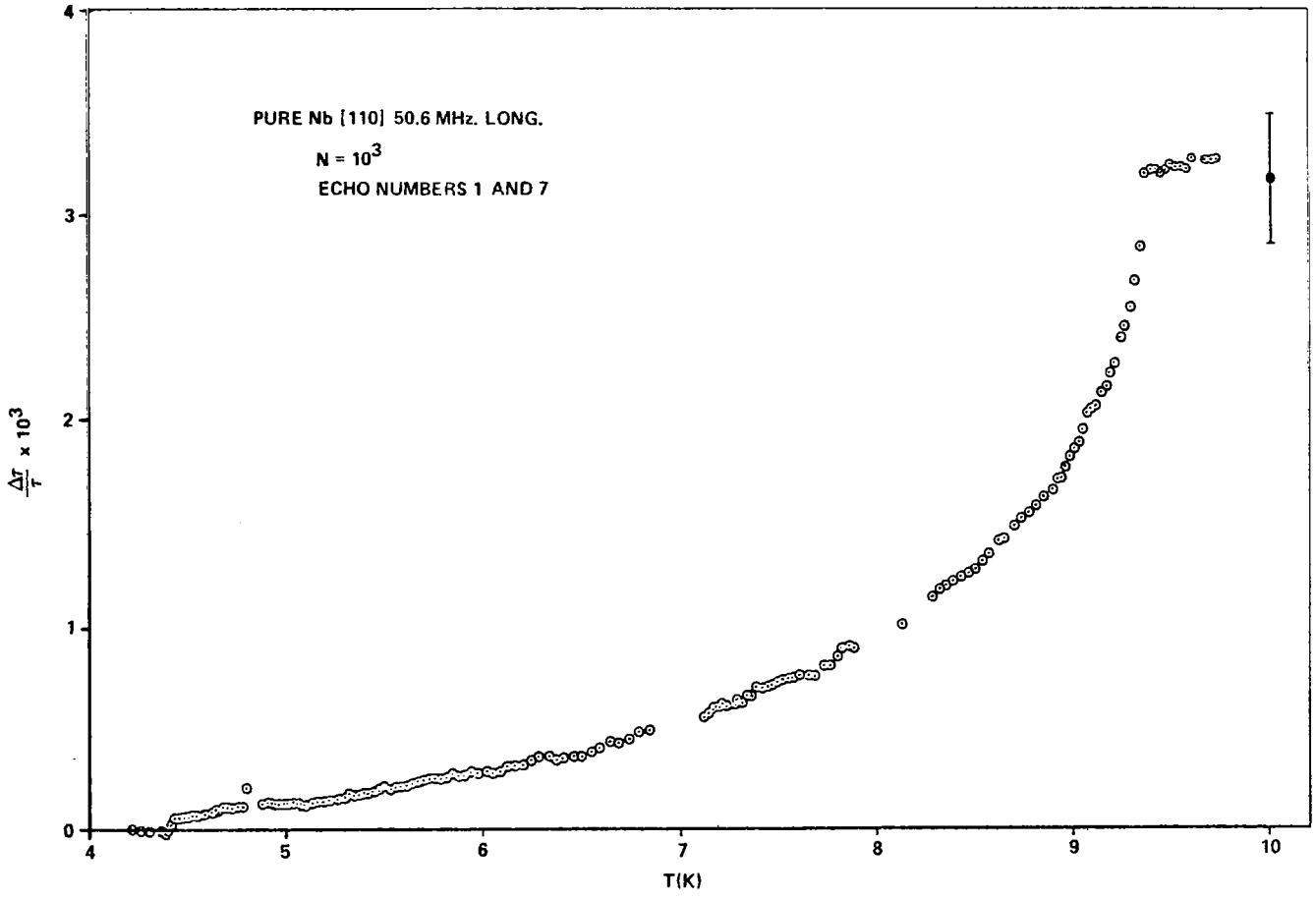

Figure 18. Fractional change in ultrasonic transit time for Nb[110] as a function of temperature.

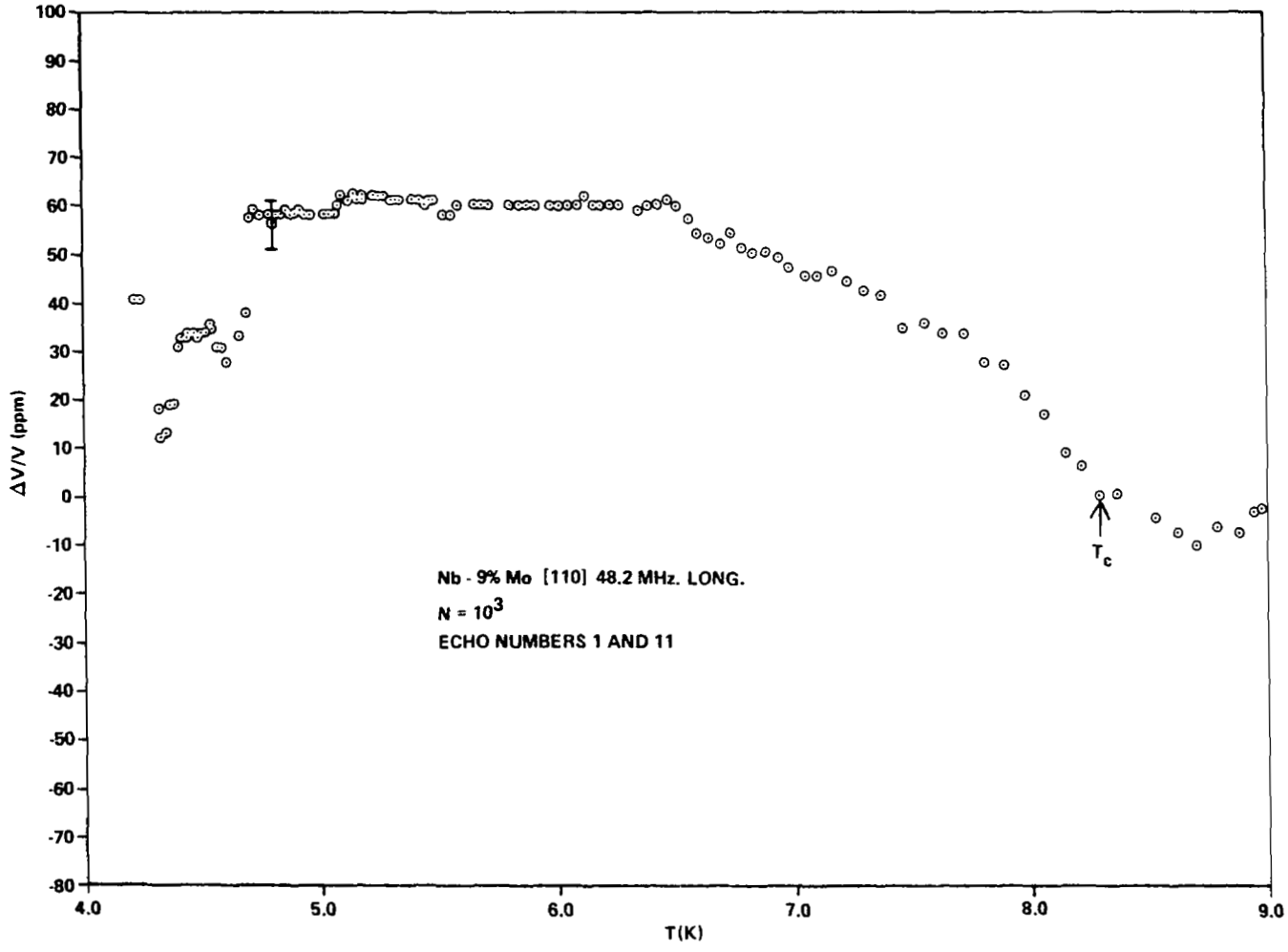

Figure 19. Fractional change in ultrasonic velocity for Nb-9%Mo[110] as a function of temperature.

where v_0 is the velocity of longitudinal waves when $\alpha_n = 0$, and M and m are the ion and electron masses, respectively. The second term is the quadratic is much less than one; therefore,

$$\frac{v_s - v_0}{v_0} = \frac{3\alpha_n^2}{8q^2} \left(1 + \frac{5Mv_0^2}{mv_F^2}\right) \quad . \tag{23}$$

For $v_F \approx 2.6 \times 10^7$ cm/s, the term in the brackets is approximately 380. From the measured α_n, we find that

$$\frac{\Delta v}{v_0} = \begin{cases} 3.4 \times 10^{-8} \text{ Nb-9\%Mo} \\ 14 \times 10^{-6} \text{ Nb} \end{cases}$$

These estimates are a factor 100 (Nb) to 2000 (Nb-9%Mo) too small to explain the data. The failure is, possibly, caused by the inability of a classical theory to explain a macroscopic quantum effect (i.e., superconductivity).

It is believed that the results can be understood in terms of an "apparent" velocity change associated with the subtleties of such a sensitive experiment. Since the attenuation of the sample is changing at the same time as the velocity is being measured, these attenuation changes will affect the velocity results. In Appendix D, this concept is used to derive the relation between the change in the transit time $\Delta\tau$ and the change in the attenuation of the sample $\Delta\alpha$:

$$\Delta\tau = 2L\,(n-m)\,\Delta\alpha\, t_r \frac{V_{tm}}{V_m} \quad , \tag{24}$$

where L is the length of the sample, n and m are the echo numbers used in the experiment, and $\Delta\alpha$ is the change in the attenuation. The effective risetime of the echos is t_r, and V_m and V_{tm} are the peak voltage and trigger voltage of echo m, respectively. Using this equation $\Delta\tau$ for Nb[110] and Nb-9%Mo[110] were calculated using an estimated $t_r = 500$ ns and the measured values of $\Delta\alpha = \alpha_n$. The error bars plotted in Figures 18 and 19 were used to show the estimated uncertainties in t_r and α_n. Excellent results have been obtained.

Before concluding this chapter, it should be noted that $\Delta\tau$ is proportional to t_r. In the modified sing-around method used by Alers [33], the apparatus is triggered directly by the rf pulse. In a 10 MHz wave $t_r = 25$ ns compared to $t_r = 500$ ns here which would give $\Delta v/v \approx 60$ ppm for the Nb sample used in this study. Alers actually obtained $\Delta v/v \approx 15$ ppm for his Nb sample which is a factor of 4 smaller than the above estimate, but it must be remembered, also, that $\Delta\tau$ is proportional to α_n and the ratio V_{tm}/V_m. Since these experimental parameters were not reported by Alers, a factor of 4 difference can still be considered as reasonable agreement between equation (24) and Alers' results. The above analysis strongly suggests that velocity measurements must be carefully analyzed in terms of the attenuation of sound in the sample.

In summary, the following conclusions and results are presented concerning the velocity measurements reported here:

1. The elastic constants in the Nb-Mo system are approximately independent of the Mo concentration; therefore, T_c is independent of the elastic constants.

2. The small velocity changes observed in a superconductor are related to the attenuation changes through equation (24).

3. The digital averaging technique[4] can be used to measure both the absolute and relative velocity of sound in solids, where two different experimental techniques were previously required.

4. The phase shift associated with sound reflection from the transducer-sample interface can be measured by the digital averaging technique.

5. The theory that relates θ_D to the elastic constants is not successful for the Nb-Mo alloys.

SECTION IV. CONCLUSIONS

The results of a rather extensive investigation of the superconducting properties of Nb and Nb-Mo alloys using ultrasonic techniques have been presented. It has been shown that the energy gap of very pure Nb is not as simple as originally found for the impure samples of the early 1960's. The need for a detailed microscopic theory to calculate the transport properties (i.e., attenuation measurements) of multiband superconductors and a possible approach to the theory (using a model which fits the experimental data of Nb) have been shown. In fact, it was found that two energy gaps were necessary to explain the attenuation of sound in pure superconducting Nb. One of the gaps, probably associated with the s electrons, is the normal energy gap given by the BCS theory with the value $A_1 = 3.4$. The other gap $A_2 = 10$ is a function of the sample purity (i.e., ℓ_e) and is much larger than that admitted by the BCS theory.

This research has shown, also, the need for a modification of the BCS theory to account for energy gaps with $A > 4$. Several theoretical papers have used the BCS theory to calculate the energy gap of strongly coupled superconductors and have found $A = 4.0$ in the strong coupling case. A modification of the BCS theory, not included here, has been developed which removes the need to artifically classify materials according to strong and weak coupling. The theory reproduces the BCS results but shows that other energy gaps are permissible. The results of the calculations indicate that the BCS theory can account for all energy gaps with $A \leqslant 4.0$. Since many energy gaps have been found experimentally with $A > 4$, the BCS theory as presently formulated is incomplete.

Measurements of the attenuation of sound in superconducting single crystals of Nb-Mo alloys have been presented. It has been shown that the interpretation of the data is difficult because of a second superconducting phase and a previously reported resonance in superconducting Nb-Mo alloys. Nevertheless, the attenuation of sound in Nb-9%Mo could be understood by assuming one energy gap with $A = 5.4$ and a second energy gap with T_{c2} of 0.35 of the T_{c1} for the first gap. Ultrasonic techniques show promise for examining the second superconducting phase of many alloys and compounds. The data on Nb-Mo alloys also indicate a need to perform additional attenuation experiments down to at least 1 K so that the second energy gap associated with the observed second phase of the alloys can be studied.

We have reported on the results of measurements of the elastic constants of Nb and two Nb-Mo alloys. The technique used to measure the elastic constants shows promise of providing an easy and accurate

4. After completing this report, the digital averaging technique was extended to include measurements on the rf with a subsequent improvement in the accuracy. A discussion of the improvements can be found in Reference 37.

technique for measuring both the absolute velocities of sound and also very sensitive changes in the velocity of sound (1 ppm). This ultrasonic technique is presently being used to study small changes in the elastic constants of alloy superconductors ($10\ K < T < 300\ K$) believed to be associated with the Kondo effect or lattice instabilities.

The digital averaging technique is applicable to a wide variety of experiments in which the velocity of sound can be studied easily as a function of a wide range of variables. It is necessary only to replace the thermometer with some other voltage-sensitive device such as a Hall probe or strain gauge. The experiment can be improved further by feeding the digital signal from the computing counter to a digital-to-analog converter which would allow an automatic plotting of the data. This technique is being adapted also to two practical engineering measuring instruments: (1) a thickness gauge designed to measure accurate thickness and surface uniformities of materials, and (2) an accurate strain gauge used to measure the strain of materials in a composite engineering structure.

George C. Marshall Space Flight Center
National Aeronautics and Space Administration
Marshall Space Flight Center, Alabama 35812, August 1971

APPENDIX A
METHOD USED TO CALCULATE α_s/α_n

In the experiment, the height Y_n was measured in volts of the nth echo as a function of temperature of the sample. Although in most of the experiments the echo pattern was strictly exponential, the more general case will be considered where nonexponential effects such as diffraction and nonparallelism may be present:

$$Y_n = Y_0 f(n) \exp(-2Ln\alpha) \quad , \tag{A-1}$$

where f(n) is some function used to describe the diffraction and wedging effects, L is the sample length, and α is the total attenuation of sound due to all effects.

Now α may be decomposed into a background attenuation α_B and the attenuation of interest:

$$\alpha = \begin{cases} \alpha_B + \alpha_n & T \geqslant T_c \\ \alpha_B + \alpha_s & T \leqslant T_c \end{cases} \quad . \tag{A-2}$$

It is generally assumed that α_B is not a function of temperature. For the present measurements and most measurements in superconductivity, this seems to be the case. Then, α_n and α_s can be expressed as functions of the Y's:

$$\alpha_n = \frac{1}{2Ln} \ln\left[\frac{Y_0 f(n)}{Y_n(T_c)} \exp(-2Ln\alpha_B)\right]$$

$$\alpha_s = \frac{1}{2Ln} \ln\left[\frac{Y_0 f(n)}{Y_n(T)} \exp(-2Ln\alpha_B)\right] \quad .$$

Therefore,

$$\frac{\alpha_s}{\alpha_n} = \frac{\ln\left[\frac{Y_0 f(n)}{Y_n(T)}\right] - 2Ln\alpha_B}{\ln\left[\frac{Y_0 f(n)}{Y_n(T_c)}\right] - 2Ln\alpha_B} \quad . \tag{A-3}$$

In the BCS theory and all ultrasonic experiments dealing with superconductors α_s is assumed to be zero at T = 0. Using this boundary condition, α_B is given by

$$\alpha_B = \frac{1}{2Ln} \ln\left[\frac{Y_0 f(n)}{Y_n(T=0)}\right] \quad . \tag{A-4}$$

Substituting equation (A–4) into equation (A–3) finally yields

$$\frac{\alpha_s}{\alpha_n} = \frac{\ln\left[\frac{Y_n(T=0)}{Y_n(T)}\right]}{\ln\left[\frac{Y_n(T=0)}{Y_n(T_c)}\right]} \qquad \text{(A–5)}$$

Note that this derivation involves the following assumptions:

1. Any echo pattern is acceptable as long as it is independent of temperature.

2. Linear amplifiers are used to measure Y_n.

3. $\alpha_s = 0$ at $T = 0$ or at the lowest obtainable temperature.

4. The background attenuation α_B is dependent of temperature.

A Hewlett-Packard 9100A computer with an X-Y plotter was used to analyze the raw data taken from X-Y plots of Y_n as a function of thermometer resistance. Equation (A–5) was derived for the case when α_n is independent of temperature such as for the Nb-9%Mo sample. If α_n is a function of temperature, as with the pure Nb sample, the more general equation can be obtained by letting $Y_n(T_c)$ assume the value $Y_n(H_{c2}, T)$.

APPENDIX B
MATERIAL CHARACTERIZATION

Resistivity Measurements

The resistivity of the cylindrical samples was determined by measuring the voltage drop across the sample due to a known current traveling through the sample. The voltage and current leads were first attached mechanically around the sample by twisting, and then good electrical contact was made by silver paint. Small currents (1 to 100 mA) were used to reduce thermal gradients and thermal emfs.

The dc voltage drop across the sample was measured with a Keithly 149 Nanovoltmeter; four or five voltages were recorded for each measurement by repeatedly reversing the current through the sample. This helped to eliminate the inaccuracies due to the thermal emfs in the circuit. The total uncertainties of the measured resistivities are believed to be 1 to 2 percent for the three different temperature ranges (300 K, 77 K, and 8 to 12 K range).

The above technique provides reliable estimates of the resistivity ratios Γ for $\Gamma < 340$. In higher Γ, other voltages in the circuit were found to experimentally decrease the signal-to-noise ratio to unity. The results for the T_c and resistivity measurements ρ are given in Table B-1.

As expected, ρ for some given temperature was linearly related to Mo concentration in the alloy single crystals and the slope of the concentration curve is dependent on the temperature. The slope of the curve increases as the temperature decreases. Figure B-1 shows $\Delta\rho/\rho_0$ as a function of Mo concentration where ρ_0 is the resistivity of pure Nb[100] and $\Delta\rho \equiv \rho(\text{alloy}) - \rho_0$. The top curve of Figure B-1 represents the data for measurements made at room temperature (300 K) and the bottom curve for liquid nitrogen results (77 K). These curves will be used in the next section to give an accurate indication of the purity of Nb single crystals.

TABLE B-1. RESISTIVITIES AND T_c OF Nb AND TWO ALLOYS OF Nb-Mo

Sample	ρ(300 K) ($\mu\Omega$-cm)	ρ(77 K) ($\mu\Omega$-cm)	ρ(10 K) ($\mu\Omega$-cm)	Γ	T_c (K)
Nb[100]	13.8	2.26		6,500	9.25
Nb[110]	14.0	2.4	0.19	74	9.13
Nb-9%Mo[110]	16.4	6.04	3.8	4.3	7.01
Nb-5%Mo[100]	15.3	4.40	2.09	11	8.06

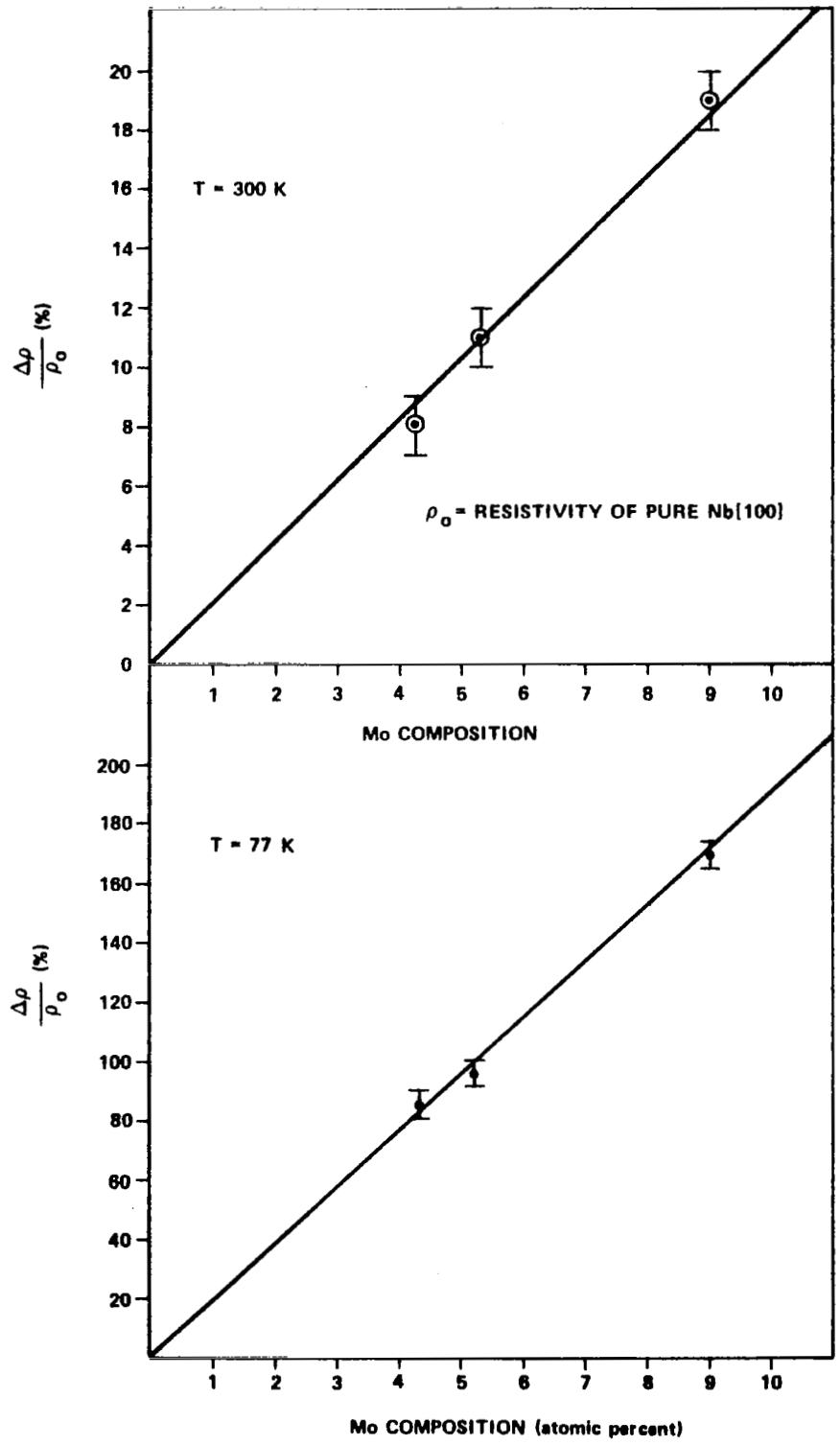

Figure B-1. Percent change in resistivity for Nb-Mo single crystals as a function of Mo compositions.

Impurity Content

The Nb[100] and Nb-5%Mo[100] crystals were obtained from Reed[5] who analyzed similar crystals by the spark emission technique. The crystals were found to have the following impurities (ppm by weight): W = 2, Ta = 15, C = 10–15, O = 5, Mo < 1, and most other metals less than 1 ppm. Total impurity content for the pure Nb varied between 50 and 75 ppm.

Using the resistivity ratio from Table B-1 and the slope from Figure B-1, a sample calculation reveals a total calculated impurity content for Nb[100] of 75 ppm which agrees with the results of the spark emission technique. It is indeed gratifying that the results of the acoustic, resistivity, spark emission and eddy current [18] techniques can be combined to yield consistent results.

T_c Measurements

The transition temperature of each sample was measured by the inductive method. This method was employed, since the dc method is ineffective for superconductors of large diameters (3 to 10 mm) and large resistivity ratios $\Gamma > 400$. In fact, for large Γ it is impossible by the dc method to determine whether the sample is normal or superconducting.

The inductive technique measures the diamagnetic transition as the sample goes from the normal state to the superconducting state. The superconductor is situated in a coil whose inductance is measured by a bridge circuit and sensitive lock-in amplifier. The lock-in amplifier provides tremendously improved signal-to-noise ratios and excellent sensitivities. This experiment was capable of detecting a few parts per million of a contaminant superconductor in our superconducting single crystals. For example, no unalloyed Nb could be detected in our Nb-Mo alloys.

As explained in Section II, the measured T_c could be used to calculate both the Mo concentration and the concentration gradients of Mo in the samples.

Determination of ℓ_e

The electron mean free paths ℓ_e for our samples were estimated from the equation derived by Pippard [34]:

$$\ell_e = 1.27 \times 10^4 \left(\rho_n N^{2/3} \, S/S_F \right)^{-1} , \qquad \text{(B–1)}$$

where ρ_n[Ω cm] is the normal state resistivity, N the conduction-electron density, and S/S_F is the ratio of the area of the Fermi surface to the area of the Fermi surface for a free-electron gas of density N. The usual assumption [35] is to let $S/S_F \approx 0.6$ for the transition metals.

---

5. R. Reed, Private Communication, Oak Ridge National Laboratory.

APPENDIX C
POSSIBLE SOURCES OF ERROR FOR ATTENUATION EXPERIMENT

Nonlinear rf Amplifiers

In any attenuation experiment, the results are strongly dependent on the linearity of the rf amplifiers. The linearity of the rf amplifiers used in this experiment was checked by two methods: (1) repetition of the experiment for various echos and (2) direct calibration of the amplifiers.

The direct test for linearity was accomplished by feeding a calibrated rf signal directly into the system at the point normally occupied by the transducer. All settings for the system were the same as for the experiment. Then the rf output of the amplifiers was read with a vector voltmeter. No nonlinear effects could be observed in the operating range of the experiment to within the calibration accuracy of the experiment (1 percent).

Equipment Calibration

All apparatus used in this experiment was calibrated periodically (3 to 6 months) by the MSFC calibration facility. As a double check on the calibration, each dc instrument was calibrated with known standard reference sources. All instruments (dc amplifiers, digital voltmeter and boxcar integrator) were within their calibration specifications.

As discussed in Section II, the germanium thermometer was calibrated with respect to a secondary standard germanium thermometer supplied by the Oak Ridge National Laboratory. The thermometer used in this experiment and other thermometers calibrated by the same technique have been used to measure the transition temperature of a variety of superconductors (Nb, V, Sn, Pb, Pb-Bi alloys, and Nb_3Sn). All the T_c agreed with published values for these materials to within 0.05 K.

Temperature Gradients Across the Sample

A simple analysis can be used to show that temperature gradients could be a source of error in rather poorly designated experiments. If the sample is not properly thermally connected to a large thermal reference source (i.e., Cu) and for large rf power levels (50 mW), the temperature gradients across the sample become severe (1 to 5 K/cm).

An experiment was performed to determine an estimated temperature gradient across the sample. First, the effective thermal conductivity of the sample holder was found by measuring its temperature increase for various known heat inputs. For heat inputs of 60 mW or less, the thermal conductivity of the sample holder was found to be 33.7 mW/K.

As a second step to the experiment, the temperature rise of the sample due to the rf power was measured as a function of the voltage setting of the rf source. This temperature rise was then used to find the maximum heat input into the sample from two sources: the direct rf power, $\dot{Q}_{rf}$, and the thermal energy, $\dot{Q}_T$, delivered to the sample from the center conductor of the coaxial cable. It was found that $\dot{Q}_{rf} = 0.34$ mW and $\dot{Q}_T = 2.8$ mW.

Using published values [36] for the thermal conductivity of Nb and assuming the worst possible case where all of the above measured heat is deposited on the top surface of the sample, the calculated maximum gradient across the Nb sample would be 0.02 K/cm at $T \approx 9$ K. This is a small gradient and probably overestimated by a factor of three. It is believed that this small temperature gradient would not significantly affect the attenuation measurements. A more detailed mathematical analysis of the effect of gradients across the sample led to the conclusion that the gradients would cause a slight underestimate of the energy gap, compared with the observed anomalies in the Nb sample which represent very large increases in the gap.

Possible Errors Associated with Uncertainties of the Echo Voltage Measurement

Using equation (A–5) derived in Appendix A, the total uncertainty associated with the normalized attenuation $d\alpha^*$, due to the uncertainties in the measured echo heights dY, is given by

$$d\alpha^* = \frac{dY/Y}{\ln(Y_0/Y_n)} \quad (3 + \alpha^*)^{1/2} \quad . \tag{C-1}$$

With the measured uncertainties of $dY/Y \leqslant 0.01$, one finds that

$$d\alpha^* = \pm 0.016 \text{ at } t \approx 1$$

$$= \pm 0.006 \text{ at } t \approx 0.5 \quad .$$

This uncertainty is a factor of 20 too small to account for the anomalous behavior of the Nb data.

APPENDIX D
APPARENT VELOCITY CHANGES DUE TO ATTENUATION CHANGES

Consider a material in which there are no true velocity changes but only changes in the attenuation of sound. For exponential echo patterns, the voltages of echo numbers n and m are related by the attenuation α:

$$V_n/V_m = \exp[-2L\alpha(n-m)] \quad . \tag{D-1}$$

Consider two superimposed triangular-shaped echos with a common base t_r (rise time) and heights V_m and V_n. The "walk" time t_w is defined as the time between the trigger voltages V_{tm} and V_{tn}, where the subscripts refer to the previous echo numbers. The "walk" time t_w can be related to the appropriate voltages:

$$t_w = t_r \left(V_{tn}/V_n - V_{tm}/V_m \right) \quad . \tag{D-2}$$

Combing equations (D-1) and (D-2) yields

$$t_w = t_r \left\{ V_{tn} - V_{tm} \exp[-2L\alpha(n-m)] \right\} / V_n \quad . \tag{D-3}$$

The interest here is not directly in the "walk" time but in the changes in the transit time $\Delta\tau$ due to changes in the attenuation $\Delta\alpha$. Since a change in the "walk" time Δt_w is equal to $\Delta\tau$, a relationship connecting $\Delta\tau$ to $\Delta\alpha$ is obtained by differentiating equation (D-3):

$$\Delta\tau = 2L(n-m)t_r V_{tm} \Delta\alpha/V_m \quad . \tag{D-4}$$

This equation relates "apparent" velocity changes to actual changes in the attenuation of sound in the sample. As shown in Section III, it accurately describes the measured velocity changes in our samples and correctly predicts the approximate amount of changes observed by other experimenters using the sing-around method.

REFERENCES

1. Bardeen, J.; Cooper, L. N.; and Schrieffer, J. R.: Phys. Rev., Vol. 108, 1957, p. 1175.

2. Bömmel, H. E.: Phys. Rev., Vol. 96, 1954, p. 220.

3. MacKinnon, L.: Phys. Rev., Vol. 98, 1955, p. 1181.

4. Kresin, V. Z.: Zr. Eksperim, i. Teor. Fiz 36, 1947 (1959) [Soviet Phys. JETP Vol. 9, 1959, p. 1385.]

5. Tsuneto, I.: Phys. Rev., Vol. 121, 1961, p. 402.

6. Ambegaokar, V.: Phys. Rev. Letters, Vol. 16, 1966, p. 1047.

7. Levy, M.: Phys. Rev., Vol. 131, 1963, p. 1497.

8. Weber, R.: Phys. Rev., Vol. 133A, 1964, p. 1488.

9. Ikushima, A.; Fujii, M.; and Suzuki, T.: J. Phys. Chem. Solids, Vol. 27, 1966, p. 327.

10. Perz, J. M. and Dobbs, E. R.: Proc. Roy. Society, Vol. 296A, 1967, p. 113. [Also see Dobbs, E.R. and Perz, J.M.: Rev. Mod. Phys., Vol. 36, 1967, p. 257 and Proceedings of 8th International Conf. on Low Temp. Phys., London, 1963, p. 195.]

11. Tsuda, N.; Koibe, S.; and Suzuki, T.: Phys. Rev. Letters, Vol. 22, 1966, p. 414.

12. Tsuda, N. and Suzuki, T.: J. Phys. Chem. Solids, Vol. 28, 1967, p. 2487.

13. McMillan, W. L.: Phys. Rev., Vol. 167, 1968, p. 331.

14. Hopfield, J. J.: Phys. Rev., Vol. 186, 1969, p. 443.

15. Deaton, B. C.: Phys. Letters, Vol. 32A, 1970, p. 333.

16. Yee, B. G. W. and Deaton, B. C.: Phys. Rev. Letters, Vol. 23, 1966, p. 52.

17. Mason, W. P.: Phys. Rev., Vol. 97, 1955, p. 557.

18. Truell, R.; Elbaum, C.; and Chick, B. B.: Ultrasonic Methods in Solid State Physics. Academic Press, New York, 1969.

19. Kaveli, M. and Wiser, N.: Phys. Rev. Letters, Vol. 26, 1971, p. 635.

20. Campbell, I. A.; Caplin, A. D.; and Rizzuto, L.: Phys. Rev. Letters, Vol. 26, 1971, p. 239.

21. Deaton, B. C.: Phys. Rev. Letters, Vol. 13, 1966, p. 577.

22. Claiborne, L. T. and Einspruch, N. G.: Phys. Rev., Vol. 151, 1966, p. 229.

REFERENCES (Concluded)

23. Garland, J. W.: Phys. Rev. Letters, Vol. 11, 1963, p. 111.

24. Claiborne, L. T. and Einspruch, N. G.: Phys. Rev. Letters, Vol. 15, 1965, p. 862.

25. Bobetic, V. M.: Phys. Rev., Vol. 136A, 1964, p. 1535.

26. Matthias, B. T.; Corenzwit, E.; Cooper, A.; and Longinotti, L.: Proceedings of the National Acad. of Sc., Vol. 68, 1971, p. 56.

27. Claiborne, L. T. and Einspruch, N. G.: Phys. Rev., Vol. 132, 1963, p. 621.

28. Chow, W. S.: Phys. Rev., Vol. 48, 1971, p. 111.

29. Konti, A. and Varshni, Y. P.: Canadian J. of Phys., Vol. 47, 1969.

30. Veal, B. W.; Hulm, J. K.; and Blaugher, R. D.: Ann. Acad. Sci. Fennicae A. VI., 1966, p. 109.

31. Baz, T. A.: Phonons and Phonon Interactions. W. A. Benjamin, Inc., New York, 1964, p. 259.

32. Steinberg, M. S.: Phys. Rev., Vol. 111, 1958, p. 425.

33. Alers, G. A. and Waldorf, D. L.: Phys. Rev. Letters, Vol. 12, 1961, p. 677.

34. Pippard, A. B.: Reports on Progress in Physics. Vol. XXXIII, The Institute of Physics and the Physical Society, London, 1960, p. 176.

35. Tittmann, B. R.: Phys. Rev., Vol. 2B, 1970, p. 625.

36. Johnson, V. J., ed.: A Compendium of the Properties of Materials at Low Temperature. Wadd Tech. Report 60-56 Part II, 1960.

37. Lacy, L. L. and Daniels, A. C.: J. Acoust. Soc. Amer., Vol. 51, May 1972.

"The aeronautical and space activities of the United States shall be conducted so as to contribute . . . to the expansion of human knowledge of phenomena in the atmosphere and space. The Administration shall provide for the widest practicable and appropriate dissemination of information concerning its activities and the results thereof."

—NATIONAL AERONAUTICS AND SPACE ACT OF 1958

NASA SCIENTIFIC AND TECHNICAL PUBLICATIONS

TECHNICAL REPORTS: Scientific and technical information considered important, complete, and a lasting contribution to existing knowledge.

TECHNICAL NOTES: Information less broad in scope but nevertheless of importance as a contribution to existing knowledge.

TECHNICAL MEMORANDUMS: Information receiving limited distribution because of preliminary data, security classification, or other reasons.

CONTRACTOR REPORTS: Scientific and technical information generated under a NASA contract or grant and considered an important contribution to existing knowledge.

TECHNICAL TRANSLATIONS: Information published in a foreign language considered to merit NASA distribution in English.

SPECIAL PUBLICATIONS: Information derived from or of value to NASA activities. Publications include conference proceedings, monographs, data compilations, handbooks, sourcebooks, and special bibliographies.

TECHNOLOGY UTILIZATION PUBLICATIONS: Information on technology used by NASA that may be of particular interest in commercial and other non-aerospace applications. Publications include Tech Briefs, Technology Utilization Reports and Technology Surveys.

Details on the availability of these publications may be obtained from:

SCIENTIFIC AND TECHNICAL INFORMATION OFFICE

NATIONAL AERONAUTICS AND SPACE ADMINISTRATION

Washington, D.C. 20546